RADAR TURBULENCE ESTIMATES: EFFECTS OF WIND SHEAR AND REFLECTIVITY FACTOR GRADIENTS

by

Stephen J. Sycuro

B.A., Richmond College

(1971)

SUBMITTED TO THE DEPARTMENT OF EARTH, ATMOSPHERIC, AND PLANETARY SCIENCES IN PARTIAL FULFILLMENT OF THE REQUIREMENTS FOR THE DEGREE OF

MASTER OF SCIENCE
IN METEOROLOGY

at the

MASSACHUSETTS INSTITUTE OF TECHNOLOGY

February 1985

Signature of Author _____
Department of Earth, Atmospheric and Planetary Sciences
February 1985

Certified by _____
Richard E. Passarelli, Jr.
Thesis Supervisor

Accepted by _____
Theodore R. Madden
Chairman, Departmental Committee on
Graduate Students

RADAR TURBULENCE ESTIMATES: EFFECTS OF WIND SHEAR AND REFLECTIVITY FACTOR GRADIENTS

by

Stephen J. Sycuro

Submitted to the Department of Earth, Atmospheric, and Planetary Sciences February 1985 in partial fulfillment of the requirements for the Degree of Master of Science in Meteorology.

ABSTRACT

Analysis of Doppler radar spectral width provides an estimate of the turbulence eddy dissipation rate (ε), which in turn can be correlated to atmospheric turbulence. The width of the Doppler spectrum provides an overestimate of the turbulence eddy dissipation rate. This overestimate may be corrected to some extent by the removal of wind shear and reflectivity factor gradients from the Doppler spectrum variance. Reflectivity factor gradients and radial velocity shears in three directions (azimuthal, vertical, and radial) are computed for points along an aircraft track. The gradient and shear effects are removed from the Doppler variance and the turbulence eddy dissipation rate is estimated using both the total and the corrected variances. Both radar estimates of the turbulence dissipation rates are then correlated with estimates of eddy dissipation rates derived from in-situ aircraft measurements. Results indicate that the only gradients significantly affecting the radar estimates are those of radial velocity shear components along the vertical or azimuthal directions. Corrections for these effects result in some improvements in the radar turbulence estimate, but the improvements are very small at the short ranges observed here. Results suggest that the gradient effects may be minor when compared to the other sources of error in the estimate of turbulence dissipation rates.

Thesis Supervisor: Dr. Richard E. Passarelli, Jr.

Title: Assistant Professor of Meteorology

TABLE OF CONTENTS

List of Tables and Figures

INTRODUCTION

Wind shear, "the local variation of the wind vector or any of its components in a given direction" (Huschke, 1959) poses a significant hazard to military and civilian aircraft. In flight, an aircraft encountering strong wind shear may be forced into a stall, be blown off a landing track, or lose enough airspeed to be forced into a dive. Obviously, these dangers are most critical during takeoffs, landings, and low-altitude flight, when the time available to recover control of the aircraft is minimal.

Aircraft turbulence, consisting of gusts, "sharp changes in wind speed relative to the aircraft; or sudden increases in airspeed due to fluctuations in the airflow, resulting in increased structural stresses on the aircraft" (Huschke) is a different type of hazard. Extreme turbulence can result in both loss of control of an aircraft and severe structural damage.

Weather forecasters can often forecast atmospheric turbulence and wind shear that may be hazardous to an aircraft, on the basis of known synoptic-scale or meso-scale atmospheric conditions. However, they cannot forecast all occurrences or precise locations of such hazards because the events are often localized and of short duration, and occur frequently with little or no prior meteorological indications. As a result, aircraft pilots still find themselves flying into hazardous conditions without warning, occasionally with disastrous results.

Most pilots can effectively control their aircraft in regions of mild turbulence. Similarly, they can maintain safe flight on entering areas of wind shear, but in both cases, forewarned is truly forearmed, and any advance warning enhances the safety factor immeasurably. Preparation for penetration into wind shear varies considerably from preparation for entering turbulence, hence, a specific warning is necessary.

How can a forecaster determine the presence of wind shear or turbulence, particularly in the large volume encompassing a region of flight? Local winds can be obtained from a meteorological tower and upper-air soundings. Pilots frequently report hazardous conditions via radio, and such pilot reports can be disseminated through a national network. These methods are helpful, but woefully inadequate, due to their very incomplete coverage.

Doppler weather radar, with its tremendous spatial sampling capability, provides a solution to the problem. In areas of measureable precipitation, Doppler radar not only provides an indication of the storm intensity, but also, through measurement of the spectrum width (the deviation of the radial velocity within the radar sampling volume from the mean radial velocity), provides an estimate of turbulent air motion intensity.

As early as 20 years ago, Rogers and Tripp (1964) discussed the application of Doppler radar techniques to the measurement of turbulence. They concluded that the time behavior of Doppler signals from snow (in particular, the spectrum width) provides a means of

estimating the total turbulent energy and the partitioning of this energy between large and small scales. Sloss and Atlas (1968) and Sloss, et al., (1969) presented further investigations, and described the effects of wind shear and reflectivity gradients on the variance of the Doppler spectrum. The earlier paper, dealing with shear of the cross-beam motion and an exponential variation of reflectivity, indicated that wind and reflectivity gradients may become significant at ranges greater than 20 km. The latter paper found the spectrum width to be essentially independent of any shear vector along the beam, that is, with radial velocity or reflectivity factors increasing or decreasing with range. Frisch and Clifford (1974) applied Doppler spectrum analysis techniques to estimate the turbulent energy dissipation rate (an indicator of atmospheric turbulence intensity) in their study of convection capped by a stable layer, and found that under most conditions radial wind shear was a negligible broadening mechanism in comparison with the broadening of the Doppler spectrum due to turbulence. Frisch and Strauch (1976) found that the effects of shear of the radial velocity on the Doppler spectrum could be removed in order to estimate the turbulent kinetic energy dissipation rates in a northeastern Colorado convective storm. Although they were unable to verify their results directly, they did find that their derived values were consistent with values measured by instrumented aircraft in other storms. Bohne (1981, 1982) has discussed the effects of imperfect precipitation response on the estimates of turbulence intensity from radar data. He found

that the Doppler spectrum variance and the estimated eddy dissipation rate are strongly dependent upon the precipitation environment for ranges less than 20 km, and in areas where the turbulence outer scale length is less than .5 km. In correlating aircraft and radar data, he found it possible to distinguish between regions of hazardous and non-hazardous turbulence with a high degree of accuracy. Labbitt (1981) also correlated aircraft and radar estimates of turbulence, and determined that the Doppler spectrum width can provide a good estimate of the turbulent field.

It is possible that intense wind shear and reflectivity gradients may introduce a significant error in the estimate of turbulence. Such an error could result in pilots receiving inexact information about the nature of the hazard they are entering. An overestimate of turbulence can cause cancellations of landings or takeoffs, while the impact of unexpected wind shear can result in serious aircraft mishaps.

It is the purpose of this report, therefor, to investigate the effects of gradients of the radial velocity and reflectivity factor on the radar estimates of turbulence severity. A technique for determining the gradients of radial velocity and reflectivity factor in three directions (azimuthal, elevation and radial), assuming a linear variation of each with direction, is presented. The effect of each gradient on the Doppler spectrum width is calculated, and removed from the total Doppler spectrum width estimates. The turbulence energy dissipation rate is estimated from the Doppler

spectrum width, with and without the gradient effects removed. The comparison of these two radar estimates of the turbulence energy dissipation rate will show the impact of gradient effects on the radar estimates. Comparison of the radar estimates with the estimates obtained from data collected by an instrumented aircraft will demonstrate whether correcting for gradient effects improves the radar estimate.

Are such effects significant in their impact on the total Doppler spectrum? If so, is it possible to delineate between wind shear and turbulence, thereby permitting specific warnings to be issued? This report seeks to provide a better understanding of the methods of estimating turbulence and wind shear through Doppler radar techniques, and thereby answer these questions, with the ultimate goal of safer flight.

THEORETICAL BASIS FOR THE EXPERIMENT

A. General Aspects of Turbulence

In any discussion of radar estimation of turbulent air motions, some basic understanding of the nature of turbulence is necessary. Tenneckes (1972) states that it is difficult to give a precise definition of turbulence, but one can list some characteristics of turbulent flows:

a) irregularity, or randomness, which requires statistical methods for analysis;

b) diffusitivity, which causes rapid mixing and increased rates of momentum, heat, and mass transfer;

c) 3-dimensional vorticity fluctuations--turbulence is rotational and 3-dimensional;

d) dissipation--turbulence tends to decay rapidly in the absence of an energy source, as kinetic energy is translated to internal energy. It is this translation of energy which enables one to estimate the intensity of the turbulent flow.

One may consider turbulence to be composed of a random collection of eddies having a range of scales (i.e., wavelengths). Then one may represent this collection as a series of harmonic functions of varying radian frequency or wavenumber, having random amplitude and combining to produce the observed turbulent structures. A wide range of length scales exists in turbulent flows. Over a limited range of scales, known as the inertial subrange, the larger scale eddies transfer kinetic energy to the

smaller scale eddies at a constant rate (ε), termed the turbulence eddy dissipation rate. This dissipation rate can be estimated from large scale dynamics which do not involve viscosity, and it is this quantity which provides a measure of the intensity of the turbulent air motions (Tenneckes, 1972). A sample of the correlation between aircraft turbulence intensity scales and the turbulent eddy dissipation rate (raised to the 1/3 power) is shown in Figure 1 (MacCready, 1964).

It is assumed throughout this report that the turbulent field is homogeneous, that is, "it is a random motion whose averge properties are independent of position in the fluid." (Batchelor, 1953). This assumes that there is no variation of the turbulent mean velocity with position, and further, that there are no variations of the average properties of the fluctuating air velocities with position (Batchelor, 1953). Also, it is assumed that the turbulence is isotropic, with properties that are independent of the axis of reference. The assumptions of homogeneity and isotropy reduce the problem of analysis to the simplest possible case, and lead to an analytical solution.

B. Aircraft Measurement of Turbulence

Labbitt (1981) states that the turbulence energy dissipation rate (ε) can be determined directly from aircraft data by simply measuring the fluctuations in instantaneous airspeed. The structure function (Dv) of the instantaneous airspeed is defined as the average of the square of the difference of two successive airspeeds, v, measured a distance, r, apart, i.e.:

$$D_V = E\{(V_2 - V_1)^2\} \quad (1)$$

and provides the turbulence energy dissipation rate (ε) through the relation:

$$D_V = C(\varepsilon r)^{2/3} \quad (2)$$

where C is a universal constant experimentally determined to be 1.77, and r is the distance between measurements of the instantaneous velocity.

The parameters measured by the aircraft to estimate the turbulence are: P_f, the static or free stream pressure; Δp, the pitot tube differential pressure; and T_t, the stagnation or total temperature. These quantities provide the means to estimate the turbulence eddy dissipation rate (ε) (Labbitt), through the relation:

$$\varepsilon^{1/3} = \frac{\left(\frac{R T_t}{\tau}\right)^{1/3} \left(\frac{\nu - 1}{2\nu}\right)^{2/3} \sqrt{D \Delta p}}{C^{1/2} \left(1 + \frac{\Delta p}{P_f}\right)^{\frac{\nu+2}{3\nu}} \left[\left(1 + \frac{\Delta p}{P_f}\right)^{\frac{\nu-1}{\nu}} - 1\right]^{2/3} P_f} \quad (3)$$

where R is the gas constant, 2.87 x 10^6 ($cm^2/sec/°K$); ν equals 1.4, the ratio of specific heats; τ is the time between successive Δp

measurements; C equals 1.77, Kolomogorov's constant; and D Δ p is the pressure structure function. The pressure structure function is the equivalent of the structure function of instantaneous velocity as described earlier:

$$D_{\Delta p} = E\{(\Delta p(t+\tau) - \Delta p(t))^2\} \qquad (4)$$

In estimating the turbulence dissipation rate, it is important to incorporate as many of the scales of turbulence present as possible. Bohne (1981) describes techniques for estimating the outer scale length from radar data, but there is an effective means of establishing, from aircraft data alone, that the majority of the scales of the turbulent field are included in the estimate of $\varepsilon^{1/3}$.

A "data segment length" is the distance traveled by the aircraft over the averaging period of the pressure structure function, D Δ p. Use of the aircraft indicated ground speed, Vag, and an arbitrarily selected data segment length, (i.e., 400 m) determines the averaging period such that the data incorporated in the structure function estimate will be centered about the desired location, thus,

Averaging period = selected data segment length/Vag
Input observations = Averaging period/# observations per second

For example, if the aircraft speed is 200 m/s and the desired data segment length is 400 m, the averaging period = 400/200 = 2 s, and the number of input observations = 24/s x 2 s = 48 observations. The 24 observations of Δ p prior to the second of interest and the 24 observations following are used for the computation of the structure function, and for the computation of the average Δ p for the averaging period.

A proper data segment length for determining the structure function at any location is found by computing estimates of the turbulence dissipation rate ($\varepsilon^{1/3}$) for a series of data segment lengths, each larger than the preceding and centered about the same location. Successive estimates of $\varepsilon^{1/3}$ will eventually approach an asymptotic value which remains relatively constant as the data segment lengths are increased. At the scale where the asymptotic value is attained, one can be assured that the data segment incorporates a sufficient range of turbulence scales so that the estimate is effectively a local ensemble average.

Figure 2 depicts the time histories of estimated $\varepsilon^{1/3}$ for the same time interval using 400 m and 1200 m data segment lengths. The marked dissimilarity between the 2 curves indicates that the 400 m data segment has not incorporated a sufficient range of turbulence scales. It is readily evident that at any given second the estimates of $\varepsilon^{1/3}$ derived from the 400 m data segment length do not approach an asymptotic value. However, a comparison of an 800 m and a 1200 m data segment length estimate yields a fairly consistent estimate of

$\varepsilon^{1/3}$. Figure 3 shows the time histories of the estimated $\varepsilon^{1/3}$ using three data segment lengths (400 m, 800 m, 1200 m) superimposed. It is quite evident that the value of $\varepsilon^{1/3}$ at any given second estimated from the use of a 1200 m data segment length is close to that estimated by the use of the 800 m segment length (within .5 cm $^{2/3}$/sec). The similarity of the estimates of $\varepsilon^{1/3}$ between the 800 m and 1200 m segment lengths indicates that these two lengths incorporate sufficient turbulence scales to allow the structure function estimates to be considered local ensemble estimates.

It is possible, of course, to continue to even larger data segment lengths. However, nothing is gained, as all future estimates will show the same structure as determined by the 1200 m length. In reality, the use of larger data segment lengths may incorporate large storm structure features which are not a part of the turbulent field, and may contaminate the structure function estimate.

C. Doppler Radar

The pulsed Doppler radar provides three spectral moments of prime importance: 1) the echo power or 0 moment of the Doppler spectrum; 2) the mean Doppler velocity or the first moment of the spectrum normalized to the zeroth moment; and 3) the spectrum width (σ_v), the square root of the second moment about the first of the normalized spectrum, a measure of velocity dispersion (Doviak, et al., 1979).

It is the spectrum width ($_v$) which enables one to estimate the strength of the turbulent air motions. The total velocity spectrum width depends upon both the radar system and meteorological parameters. Most effects due to the radar system parameters (e.g., beamwidth, pulsewidth, etc.) can be removed in the original data analysis. Then, assuming the meteorological spectral broadening parameters are independent of each other, the total Doppler spectrum width can be treated as a sum of variances (σ^2) due to each parameter (Doviak, et al., 1979)

$$\sigma^2_v = \sigma^2_s + \sigma^2_r + \sigma^2_d + \sigma^2_t \qquad (5)$$

where: σ^2_v = total spectrum variance (width squared)

σ^2_s = portion of variance due to wind shear

σ^2_r = portion of variance due to rotation of the antenna (beam sweeping through space is sampling different targets)

σ^2_d = portion of variance due to differences in particle fall speeds

σ^2_t = portion of variance due to turbulent air motions.

Various investigators (Frisch and Clifford, 1974, Frisch and Strauch, 1976, Doviak, et al., 1979) have concluded that at low elevation angles (< 15°) there are two dominant factors contributing to the Doppler spectrum variance: wind shear and turbulence. Therefore, the total spectrum variance may be written

$$\sigma_v^2 = \sigma_t^2 + \sigma_s^2 \tag{6}$$

where

$$\sigma_s^2 = \sigma_\theta^2 + \sigma_\phi^2 + \sigma_r^2 \tag{7}$$

where σ^2_θ = due to shear in azimuthal direction

σ^2_ϕ = due to shear in the vertical direction

σ^2_r = due to shear in the range direction

It is relatively simple to compute the radial velocity gradients about a specified point (the beam center) by assuming a linear velocity field so that

$$V_r = V_o + K_1 r\phi + K_2 r\theta + K_3 h \tag{8}$$

where: V_r = radial velocity at any location

V_o = reference radial velocity at the center of the beam

k_1, k_2, k_3 = gradients of the radial velocity in the ϕ, θ, h directions respectively

ϕ = elevation angle from the beam center

θ = azimuthal angle from the beam center

h = range distance from the beam center

A least-squares fitting operation is performed on the radial velocity

values within a sphere about the reference point to satisfy the matrix operation

$$\begin{pmatrix} \sum r^2\phi^2 & \sum r\phi r\theta & \sum r\phi h \\ \sum r\theta r\phi & \sum r^2\theta^2 & \sum r\theta h \\ \sum r\phi h & \sum r\theta h & \sum h^2 \end{pmatrix} \begin{pmatrix} K_1 \\ K_2 \\ K_3 \end{pmatrix} = \begin{matrix} \sum (V-V_o) r\phi \\ \sum (V-V_o) r\theta \\ \sum (V-V_o) h \end{matrix} \qquad (9)$$

Solutions for k_1, k_2, k_3 are determined through a simple matrix inversion.

Sloss and Atlas (1968), and Atlas et al. (1969), have discussed not only the effects of wind shear on Doppler radar spectra, but have also discussed the effects of reflectivity factor gradients. In the earlier paper, shear of the cross-beam motion is considered, while the later paper deals with the component of shear along the beam. Here we combine both cross beam and along beam gradients of velocity and reflectivity factor. Assuming these linear variations, one is able to derive analytical expressions for the effects of gradients on the central moments of the Doppler spectrum. The analysis is described below. First, as with velocity (eq. 8), a linear variation of reflectivity factor in dBz (10 log Z) is used

$$dBz = dBz_o + Q_1 r\phi + Q_2 r\theta + Q_3 h \qquad (10)$$

where dBZ_0 = reflectivity factor at the beam center, and Q_1, Q_2, Q_3 are gradients in dBz in ϕ, θ, h, direction (dBz/km). Secondly, the Z variation is represented exponentially

$$Z/Z_o = \exp(b_1 r\phi + b_2 r\theta + b_3 h) \tag{11}$$

where $b_1 = (\ln 10)/10\ Q_1 = .23\ Q_1$, $b_2 = .23\ Q_2$, and $b_3 = .23\ Q_3$. A Gaussian beam pattern is assumed

$$I/I_o = \exp\left(-\alpha\left(\phi^2/\phi_o^2 + \theta^2/\theta_o^2\right)\right) \tag{12}$$

where ϕ_o, θ_o are the 1/2 power full beam widths for the one way transmission. Since I/Io refers to the two way pattern ϕ_o, θ_o are the 1/4 power points, i.e., for $\theta = 0$, $\phi = \phi_o$, I/Io = 1/4 = exp $(-\alpha)$, $\alpha = \ln 4 = 1.386$. The expression for the nth moment of the Doppler spectrum is

$$\overline{V^n} = \frac{\int_{-\infty}^{\infty}\int_{-\infty}^{\infty}\int_{-H/2}^{H/2} V^n \frac{I(\phi,\theta)}{I_o}\frac{Z(\phi,\theta,h)}{Z_o}\,dh\,d\theta\,d\phi}{\int_{-\infty}^{\infty}\int_{-\infty}^{\infty}\int_{-H/2}^{H/2} \frac{I(\phi,\theta)}{I_o}\frac{Z(\phi,\theta,h)}{Z_o}\,dh\,d\theta\,d\phi} \tag{13}$$

with v, I, Io, Z/Zo as previously defined. The variance is simply $\sigma^2_v = \overline{V^2} - \overline{V^1}^2$, so it is simply necessary to compute the two moments $\overline{V^1}$ and $\overline{V^2}$, square and subtract $\overline{V^1}$ from $\overline{V^2}$. Beginning with

$$V^J = (V_0 + k_1 r\phi + k_2 r\theta + k_3 h)^J \tag{14}$$

One proceeds with simple binomial expansion theorems through

$$V^J = \sum_{m=0}^{J} \binom{J}{m} V_0^{J-m} (k_1 r\phi + k_2 r\theta + k_3 h)^m$$

$$= \sum_{m=0}^{J} \sum_{L=0}^{m} \binom{J}{m}\binom{m}{L} V_0^{J-m} (k_1 r\phi)^{m-L} (k_2 r\theta + k_3 h)^L \tag{15}$$

$$= \sum_{m=0}^{J} \sum_{L=0}^{m} \sum_{K=0}^{L} \binom{J}{m}\binom{m}{L}\binom{L}{K} V_0^{J-m} (k_1 r\phi)^{m-L} (k_2 r\theta)^{L-K} (k_3 h)^K$$

to

$$V^J = \sum_{m=0}^{J} \sum_{L=0}^{m} \sum_{K=0}^{L} \binom{J}{m}\binom{m}{L}\binom{L}{K} V_0^{J-m} k_1^{m-L} k_2^{L-K} k_3^K r^{m-K} \phi^{m-L} \theta^{L-K} h^K \tag{16}$$

and finally

$$\widetilde{V^J} = \sum_{m=0}^{J} \sum_{L=0}^{m} \sum_{K=0}^{L} \binom{J}{m}\binom{m}{L}\binom{L}{K} V_0^{J-m} k_1^{m-L} k_2^{L-K} k_3^K r^{m-K}$$

$$\left[\int_{-\infty}^{\infty}\int_{-\infty}^{\infty}\int_{-H/2}^{H/2} \exp\left(-\frac{\alpha\phi^2}{\phi_0^2} + b_1 r\phi\right) \exp\left(-\frac{\alpha\theta^2}{\theta_0^2} + b_2 r\theta\right) \exp(b_3 h) \right. \tag{17}$$

$$\left. \cdot \phi^{m-L} \theta^{L-K} h^K \, dh\, d\theta\, d\phi \right]$$

$$\Big/ \int_{-\infty}^{\infty}\int_{-\infty}^{\infty}\int_{-H/2}^{H/2} \exp\left(-\frac{\alpha\phi^2}{\phi_0^2} + b_1 r\phi\right) \exp\left(-\frac{\alpha\theta^2}{\theta_0^2} + b_2 r\theta\right) \exp(b_3 h)\, dh\, d\theta\, d\phi$$

At this point it is possible, though tedious, to calculate V by summing through the indices. (See Gradsteyn, pp 92, 307, 337). The first result is

$$\bar{V} = V_0 + \frac{r^2}{2\alpha}\left(K_1 b_1 \phi_0^2 + K_2 b_2 \theta_0^2\right)$$

$$- \frac{K_3}{b_3} + \frac{HK_3}{2}\left(\frac{1+e^{-b_3 H}}{1-e^{-b_3 H}}\right) \qquad (18)$$

A similar procedure, applying the same formulae, yields

$$\overline{V^2} = V_0^2 + \frac{V_0 r^2}{2\alpha}\left[K_1 b_1 \phi_0^2 + K_2 b_2 \theta_0^2\right] - \frac{2V_0 K_3}{b_3} + V_0 H K_3\left[\frac{1+e^{-b_3 H}}{1-e^{-b_3 H}}\right]$$

$$- \frac{r^2 K_3}{\alpha b_3}\left[K_1 b_1 \phi_0^2 + K_2 b_2 \theta_0^2\right] + \frac{HK_3 r}{2\alpha}\left[K_1 b_1 \phi_0^2 + K_2 b_2 \theta_0^2\right]\left[\frac{1+e^{-b_3 H}}{1-e^{-b_3 H}}\right]$$

$$- \frac{HK_3^2}{b_3}\left[\frac{1+e^{-b_3 H}}{1-e^{-b_3 H}}\right] + \frac{r^4}{4\alpha^2}\left[K_1 b_1 \phi_0^2 + K_2 b_3 \theta_0^2\right] \qquad (19)$$

$$+ \frac{K_3^2}{b_3^2} + \frac{H^2 K_3^2}{4}\left[\frac{1+e^{-b_3 H}}{1-e^{-b_3 H}}\right]^2$$

This reduces to

$$\sigma^2 = \frac{r^2}{2\alpha}\left[K_1^2 \phi_0^2 + K_2^2 \theta_0^2\right] + \frac{K_3^2}{b_3^2}$$

$$-K_3^2 H\left[\frac{e^{-b_3 H}}{(1-e^{-b_3 H})^2}\right] \qquad (20)$$

In the case where $b_3 = 0$, the integration terms are modified with the result that

$$\bar{V} = V_0 + \frac{r^2}{2\alpha}\left(K_1 b_1 \phi_0^2 + K_2 b_2 \theta_0^2\right) \qquad (21)$$

and

$$\overline{V^2} = V_o^2 + \frac{V_o r^2}{\alpha}\left[K_1 b_1 \phi_o^2 + K_2 b_2 \theta_o^2\right]$$

$$+ \frac{r^4}{2\alpha^2}\left[K_1 b_1 K_2 b_2 \phi_o^2 \theta_o^2\right] + \frac{r^4}{4\alpha^2}\left[K_1^2 b_1^2 \phi_o^4 + K_2^2 b_2^2 \theta_o^4\right] \qquad (22)$$

$$+ \frac{r^2}{2\alpha}\left[K_1^2 \phi_o^2 + K_2^2 \theta_o^2\right] + \frac{K_3^2 H^2}{12}$$

and finally

$$\sigma^2 = \frac{r^2}{2\alpha}\left(K_1^2 \phi_o^2 + K_2^2 \theta_o^2\right) + \frac{K_3^2 H^2}{12} \qquad (23)$$

Note the absence of b_1, and b_2 in the final equations, indicating that the independent gradients of reflectivity factor in the azimuthal and elevation directions have no effect on the Doppler spectrum width.

It is possible to compute some representative values of the effects of gradients in radial velocity and reflectivity factor on the Doppler spectrum width. The following assumptions and conditions apply: 1) the beam pattern is assumed to be Gaussian along both the radial and transverse directions; 2) the full half-power beam width is 1.5 degrees; 3) the pulse depth is 150 m; 4) the reference radial velocity at the center of the beam, Vo, is 10 m/s.

Under these conditions, the application of equations (20) and (23) to various values of radial velocity shear and reflectivity

factor gradients, at different ranges, yields the results indicated in Table 1. The values of k_1 (radial velocity changes with elevation), k_2 (radial velocity changes with azimuth), k_3 (radial velocity changes along the radial), and b_3 (reflectivity factor gradients along the radial), are arbitrary values, used here only to demonstrate the effects of these quantities on the Doppler spectrum width. The Doppler spectrum width due to the gradients is computed at ranges of 25, 50, and 75 km, to demonstrate the range dependence.

The results indicated in Table 1 are fairly simple to describe intuitively. For a given shear of the radial velocity transverse to the beam, the difference in the velocities across the beam will be larger when the beam width is large, resulting in a larger spectrum width. Since the range and half-power beam width determine the distance across the beam, it is logical that the spectrum width will depend directly on these two values. Similarly, the effect on the spectrum width due to radial velocity shear or reflectivity factor gradients along the beam should be minimal, because even with reasonably large gradients, the range of velocities over the short pulse volume depth of 150 m will be very small.

It must be noted again that a linear variation of the radial velocity and of the log of the reflectivity factor are assumed in the preceding. The gradients of the log of the reflectivity factor are computed in the same manner as the velocity gradients. With these assumptions, it is now possible to subtract that portion of the Doppler spectrum variance due to radial wind and reflectivity factor

gradients from the total variance to determine the spectrum variance due to turbulence alone:

$$\sigma^2_t = \sigma^2_v - \sigma^2_s \qquad (24)$$

The Doppler spectrum width provides the means for estimating the turbulence eddy dissipation rate (ε) from radar data (Labbitt). Assuming isotropic homogeneous turbulence, that the turbulence field may be modeled as inertial subrange in form, and assuming the radar beamwidth is much larger than the pulse length, the relation between the turbulence eddy dissipation rate and the Doppler velocity spectrum width is:

$$\varepsilon^{1/3} = \frac{\sigma^2_v}{\sqrt{1.828}\, a^{1/3}} \qquad (25)$$

where ε is the eddy dissipation rate, σ^2_v is the Doppler spectrum width, and a is the radar half-beam width.

Note that Labbitt neglects wind shear and reflectivity factor gradients, and uses the entire spectrum width to estimate the turbulence eddy dissipation rate. It is assumed that a better estimate of $\varepsilon^{1/3}$ may be obtained if the gradient effects on the Doppler spectrum variance are removed. Hence, where Labbitt uses the total radar-estimated variance, σ^2_v, to estimate $\varepsilon^{1/3}$, here the variance due to turbulence alone (the result of subtracting gradient contributions from the total) is used, with the result that equation

(25) is changed to:

$$\varepsilon^{1/3} = \frac{\sigma_t^2}{\sqrt{1.828}\, a^{1/3}} \qquad (26)$$

where, instead of the total width σ_v the computed width due to turbulence alone, σ_t, is used in the estimate of $\varepsilon^{1/3}$.

DESCRIPTION OF THE EXPERIMENT

The Lincoln Laboratory Summer-83 Project combined the collection of meteorological data by an instrumented University of North Dakota Citation II aircraft, flying planned routes through precipitation, with the simultaneous collection of radar data by the Massachusetts Institute of Technology WR66 (10 cm) Doppler radar.

The inertial navigation system aboard the aircraft provided the aircraft location (latitude, longitude, altitude (MSL) at intervals of one second (measured as seconds from midnight). The aircraft did not measure gust velocities; however, all significant quantities necessary for an estimate of $\varepsilon^{1/3}$ (pitot-static pressure, static pressure, temperature) were recorded as functions of time.

Aircraft data were recorded at rates of 1 observation per second (every .98304 sec, T1 data), and approximately 24 observations per second (every .04096 sec, T24 data). Some of the T1 data are actually the numerical averages of observations taken at the rate of 24 per second.

The T1 data were used to determine the aircraft location at each second. The aircraft true heading was extracted to determine the time intervals of straight "runs" of the aircraft. Aircraft ground speeds (Vag) obtained from the T1 data established the averaging period (for the selected data segment lengths) for the structure function analysis of the pitot-tube pressure data. All latitudes, longitudes, and altitudes were converted to a spherical coordinate system (elevation, azimuth, range) centered at the radar location.

The T24 data provided total temperature (T_t), differential pitot-tube pressure (Δp), and the static pressure (P_f) for estimation of the turbulence eddy dissipation rate (ε).

Although the radar was not slaved to the aircraft during the aircraft penetrations, sector volume scans through the regions penetrated by the aircraft were collected. The radar data provided the reflectivity factor, Doppler velocity, Doppler spectrum width, and total turbulence eddy dissipation rate (based on the total variance values, without gradient effects removed) for points in the vicinity of the aircraft. MIT Testbed Radar characteristics are listed in Appendix A.

NOTE: Both aircraft and radar data tapes, and the programs to decode the tapes, were provided by Lincoln Laboratory, MIT. Basic equations and algorithms used in decoding the tapes are listed in Appendix B.

The aircraft made two flights on 12 August 83, one in the morning (10:00-13:40 EDT) and one in the afternoon (14:30-16:45 EDT). A low pressure system was situated in southern New York state, and moved eastward throughout the day. North and east of the low, there were stratiform clouds with rain and rainshowers extending from New York to Maine. Surface winds were northeasterly at 5-10 knots, while winds at the 700 millibar level were southwesterly at approximately 30 knots. Temperatures ranged from 56° F to 69° F in

the Boston area. Satellite data indicate that there was thunderstorm activity associated with the system, however, the aircraft did not fly in the vicinity of the thunderstorms during the experiment.

Figures 4 through 11 show the reflectivity factor and velocity fields interpolated to constant altitude surfaces at 12:59 and 16:35 EDT. The times listed here and on the figures represent the starts of the volume sector scans which provided the data for the plots. A 3-dimensional interpolation scheme is used to interpolate data to grid points spaced at intervals of two kilometers. Note that the figures show only the area west of the radar (azimuth 180°-360°), those areas encompassing the regions of storm penetration by the aircraft.

Figures 4-7 depict the reflectivity factor fields at the heights indicated (2 and 3 km for the morning flight, 1 and 2 km for the afternoon flight), at the times indicated. The track of the aircraft is superimposed on the figures. It is obvious from these figures that noticeable reflectivity factor gradients in all three directions (elevation, azimuth, and radial) are present ($\pm$ 10 dBZ/km).

Similarly, Figures 8-11 show marked radial velocity gradients ($\pm$ 8 m/s/km). The combined conditions of notable radial velocity and reflectivity factor gradients makes this an excellent case for analyzing their effects on radar spectra.

The aircraft made several straight runs through the areas of precipitation for each flight. For reasons to be discussed later,

not all of the runs could be analyzed and compared with radar data. Figures 12 and 13 are the time histories of the estimated $\varepsilon^{1/3}$ for the two runs analyzed. These time histories contain 3 estimates of $\varepsilon^{1/3}$, each based on data segment lengths of 400 m (long dashes), 800 m (short dashes), and 1200 m (solid). The time histories of the 800 and 1200 meter data segment lengths are similar in structure and differ greatly from the time history based on the shorter (400 m) data segment length. This demonstrates that with the increasing data segment length the estimate of $\varepsilon^{1/3}$ is approaching an asymptotic value at each second, and one may assume that the 1200 m data segment length has incorporated most of the scales of the turbulent motion. The estimates of $\varepsilon^{1/3}$ based on the 1200 m data segment length are considered ground truth for correlation with the radar estimates of $\varepsilon^{1/3}$.

A difficult problem arises when one attempts to correlate aircraft and radar data, in that it is frequently difficult to spatially and temporally co-locate the two data sets. At any given second, the aircraft is located at a particular position while the radar may be scanning a completely different sector.

It is inappropriate to simply ignore the time differences and choose the beam center closest to the aircraft location as a reference point, because even over short time intervals (i.e., 5 minutes) significant changes may occur in both the storm radial velocity and the reflectivity factor fields. Similarly, it is necessary to accept only limited spatial regions while correlating in

time, in order to maintain commonality of the storm features observed by the aircraft and radar. As a result of these restrictions, data from several aircraft runs were eliminated, as the radar data were not within predetermined temporal and spatial bounds.

An even more critical problem arises in the attempt to co-locate the data sets if there are errors in the aircraft or radar location measurements. For example, a typical value for the error in the inertial navigation system, radar location, or in the interpolation to range, azimuth and elevation may be as much as 1 km. It is necessary in the data processing scheme to establish a radar reference point, which is the radar data point closest to the aircraft location, in order to determine Vo, dBZo, etc. An aircraft-radar location error of 1 km implies that any number of radar data points within a kilometer of the nominal aircraft location could be the correct reference point. Even if this problem were non-existent, there are further complications due to the time lag between the two data sources, which, when combined with the effects of advection and evolution of the storm features, seriously degrades the correlation between the aircraft data and the radar reference point data. An attempt to simply use the radar data point geographically closest to each particular aircraft location was quite unsuccessful. That is, the values of the radar estimate of $\varepsilon^{1/3}$ taken from the radar data point closest to the aircraft track showed no correlation with the aircraft estimated $\varepsilon^{1/3}$.

Appendix C describes an alternate method for determining the radar reference points to be used. The entire radar derived turbulence dissipation rate is interpolated to a 2-dimensional field at the aircraft altitude. Hypothetical aircraft tracks, based on the nominal track indicated, are superimposed on the radar-derived field and the cross-covariance for the aircraft and radar estimates of $\varepsilon^{1/3}$ are computed for each track. The cross-covariance values indicate the possible best-fitting aircraft tracks. Final selection of a single track is made after a comparison with observed features (advection by upper level wind, evolution). For both of the runs of August 12, a shift of 2.5 km north and 2.5 km east of the original track provided the best results. The 700 millibar winds were from the south-southwest at approximately 30 knots. Hence, one expects that the radar data field, measured prior to the aircraft penetration, would be shifted to the north and east at the time of the aircraft passage. This alternate process provided a reasonable correlation between aircraft and uncorrected radar data, and the data set of reference points to be analyzed for gradient effects.

Once the radar reference points are determined the radar data are screened again, to select the 125 (if possible) nearest radar data points about each designated radar reference point. A distance limit about the designated radar reference point (where distances are the straight-line point-to-point distances) of 1 km determined the points to be accepted in the calculation of radial velocity shear and reflectivity factor gradients.

The points within the 1 kilometer sphere about the designated radar reference point (representing the aircraft location) are processed through the matrix inversion described in part 2 to determine the gradients in radial velocity and reflectivity factor. The computed gradients become the input to the program which returns the effects on the radar spectrum variance due to radial velocity and reflectivity factor gradients (σ^2_s). These effects are subtracted from the radar-estimated total variance (σ^2_v), and the remaining variance due to turbulence alone (σ^2_t) provides the means, through equation 26, for the estimation of the turbulence dissipation rate ($\varepsilon^{1/3}$). Figure 14 presents a block diagram of the entire data-processing technique. The final output is a listing of the gradients of radial velocity and reflectivity factor, $\varepsilon^{1/3}$ estimates from the aircraft data, $\varepsilon^{1/3}$ estimates from the total radar measured variance, and $\varepsilon^{1/3}$ estimates from the radar measured variance due to turbulence alone, all correlated to the time interval of the aircraft penetration.

Reference to Figures 12, 13, and to Figure 1 (MacReady) indicates that the turbulence ranged from negligible to moderate in intensity, with a few periods of heavy turbulence.

RESULTS

Figures 15-20 display time histories of the turbulence eddy dissipation rates, reflectivity factor gradients, and radial velocity gradients for the two aircraft runs. Figures 15 and 18 depict the aircraft-estimated $\varepsilon^{1/3}$ (large dashes), the radar estimated $\varepsilon^{1/3}$ without gradient effects removed (small dashes), and the radar estimates with gradient effects removed (solid). Both radar estimates are considerably higher than each aircraft estimate, although the time histories display the same trends of variation.

The discrepancy between the radar-derived estimates of $\varepsilon^{1/3}$ and the aircraft estimates may be due to a variety of factors. Two factors, the shear of the mean Doppler velocity and gradients of the reflectivity factor, have already been removed. Other factors include the antenna rotation speed, side-lobe contamination, non-Gaussian and bimodal spectra, radar biases resulting from amplitude/phase imbalances, and the assumption of a 3-dimensional homogeneous isotropic field.

While it is difficult to verify the presence of all of the factors listed, it is possible to gain some sense of their possible effects. The contribution of the antenna rotation speed to the Doppler spectrum width is extremely small. Side-lobe contamination could cause a significant overestimate of $\varepsilon^{1/3}$ in regions where the aircraft is near a high reflectivity area. However, it is difficult to gain a quantitative estimate of this effect; there is no apparent correlation between the path of the aircraft through the reflectivity

field and the magnitude of the discrepancy throughout the time history. Non-Gaussian or bi-modal spectra were determined to be factors in the overestimates of turbulence in the Labbitt paper. Such effects may definitely contribute to the discrepancies, but generally would occur only at specific points, and can not account for the consistent overestimates throughout the entire period. Bohne also found that even after the removal of effects due to shear of the radial velocity and Doppler spectral contaminants, such as image spectra, the radar estimates of turbulence in areas of light to low moderate turbulence were significantly higher than the aircraft estimates. It is not possible to determine the quantitative effects of radar biases; however, it should be noted that such biasing would produce an effect that would persist throughout the entire period of the run.

The assumption of a 3-dimensional homogeneous isotropic turbulent field may be in error. For example, consider the extreme case where the turbulence field was actually 2-dimensional. This discrepancy field may produce a significant error which may, under certain assumptions, be quantitatively estimated. When the pulse volume is much larger than the largest turbulent eddy, then the turbulence motions are mapped almost entirely into the Doppler spectrum variance. Thus the variance would be $\overline{v'^2}$, (assuming $\overline{v'} = 0$, where v' is the gust velocity along the radial direction). Assume the turbulence energy density is described by the Kolmogorov relation

$$\tfrac{1}{2}\left(\overline{u'^2} + \overline{v'^2} + \overline{w'^2}\right) = \int C\,\varepsilon^{2/3} K^{-5/3}\, dK \qquad (27)$$

where $\overline{u'^2}$, $\overline{v'^2}$, $\overline{w'^2}$ are the mean square turbulence fluctuations along three orthogonal directions, C is a known constant, and K is the magnitude of the turbulence wave vector $(\vec{K})$.

The assumption of 3-dimensional homogeneous isotropic turbulence results in $\overline{u'^2} = \overline{v'^2} = \overline{w'^2} = \langle var \rangle$, yielding

$$\tfrac{3}{2}\langle VAR\rangle = \int C\,\varepsilon^{2/3} K^{-5/3}\, dK \qquad (28)$$

Now if the field is actually two dimensional in nature, the energy equation becomes

$$\tfrac{1}{2}\left(\overline{u'^2} + \overline{v'^2}\right) = \int C\,\varepsilon^{2/3} K^{-5/3}\, dK \qquad (29)$$

assuming that the energy density takes the same form as indicated previously. Again, assuming $\overline{u'^2} = \overline{v'^2} = \langle var \rangle$ then, for the two dimensional field, the result is

$$\langle VAR\rangle = \int C\,\varepsilon^{2/3} K^{-5/3}\, dK \qquad (30)$$

To compare the 2 cases the relations are related by

$$\varepsilon^{1/3}_{(3d)} = \sqrt{3/2}\;\; \varepsilon^{1/3}_{(2d)} \qquad (31)$$

Where $\sqrt{3/2}$ = 1.22. Note that a given variance yields a value of $\varepsilon^{1/3}$ in an assumed 3-dimensional field that is 22% larger than what it would yield if the field were actually a two dimensional field. Thus the assumption of the existence of a 3-dimensional field where actually a 2-dimensional field is present could lead to a consistent 22% overestimate.

It is reasonable to conclude that some combination of the above factors tends to produce the overestimates of $\varepsilon^{1/3}$. It is also possible that some aircraft bias may have resulted in lower turbulence dissipation rates than actually existed in the field. Although the radar estimates of $\varepsilon^{1/3}$ are much higher than the aircraft values, the experimental results still provide valuable information about the effects of gradients on the turbulence estimates.

Figure 16 displays the reflectivity factor gradients in each direction, with b_1 indicated by small dashes, b_2 by solid lines, and b_3 by the large dashes. As determined previously the only reflectivity factor gradient of interest is b_3. There is no discernible relation between the time history of b_3 and that of the radar estimated $\varepsilon^{1/3}$. That is, at those points where the radar estimates diverge there is no significant change in b_3. This result agrees with those of Table 1, corroborating the minimal effect of the gradient in the reflectivity factor along the radial direction.

Figure 17 shows the gradients of velocity along each direction, with k_1 indicated by the small dashes, k_2 by the solid line, and k_3

by the large dashes. There is little correlation between the divergence of the radar estimates and the time history of k_3, which agrees with the theoretical results of Table 1, that radial velocity gradients along the radial direction have little effect on the Doppler spectrum width.

Note, however, the significant change in k_1 at approximately t = 30s. As this quantity increases in magnitude, the spread between the two radar estimate of $\varepsilon^{1/3}$ increases, to a maximum at t = 70s. As the velocity gradient approaches 0.0 at t = 80, the two radar estimates coincide, then diverge again as the gradient increases. In this particular case, there is a very obvious correlation between the k_1 (vertical) velocity gradient and the radar estimates of $\varepsilon^{1/3}$.

Figures 18, 19, 20 display the time histories of the quantities of interest for the afternoon run. As in Figure 15, Figure 18 shows the radar-derived estimates of $\varepsilon^{1/3}$ following but still larger than the aircraft estimates. Also, the differences between the radar estimates without gradient effects removed and those with gradient effects removed is so small that the two plots overlap, indicating an extremely small change in the estimate. However, other results are evident in the plots.

Figure 19, the reflectivity factor gradient time history, shows major changes in the magnitude of b_3. These changes are not reflected in the radar estimates of $\varepsilon^{1/3}$ (no divergence of the estimates), again showing the minimal effects of the reflectivity factor gradients along the radial on the Doppler spectrum width.

Figure 20 indicates little change in the verocity gradients throughout the time interval. The k_3 gradient (along the radial) shows the largest magnitude and greatest variability, but, as determined previously, this component of the radial velocity shear has little effect on the variance. Further, the low magnitudes of the k_1 and k_2 shears throughout the time interval are reflected in the very close values of the two radar estimates. That is, the small differences between the two radar estimates would have been predictable on the basis of the low shear component values.

Another feature of the results depicted by Figures 15 and 18 is the distance of the aircraft track from the radar. Equations 21 and 24 explicitly show the range dependence of the variance due to shear--for given magnitudes of shear, a doubling of the range results in a quadrupling of the shear effects. Since the morning track (Fig. 15) is at an approximate range of 50 km while the afternoon track (Fig. 18) is at approximately 25 km, one expects that the differences between the two radar estimates will be greater for the morning run (at the larger range), assuming comparable range scale gradients at each range.

The cross-covariances of the aircraft and radar estimates of $\varepsilon^{1/3}$ (for radar estimates with and without gradient effects removed) are indicated below:

Data sets:	Cross-covariance
am, aircraft and radar without gradient effects removed.	.6028
am, aircraft and radar with gradient effects removed.	.6055
pm, aircraft and radar without gradient effects removed.	.6819
pm, aircraft and radar with gradient effects removed.	.6834

As indicated above, there is little improvement in the correlation of the aircraft and radar estimates by removing the effects of the gradients from the Doppler spectrum variance. In both cases, estimates of $\varepsilon^{1/3}$ derived from the radar data tend to overestimate the turbulence by such a large amount that removing the gradient effects is of little consequence for these particular data.

CONCLUSION

There is no doubt that radial velocity shear and reflectivity factor gradients affect the width of the Dopler spectrum. The combined effects can be determined and isolated, assuming a linear variation in the radial velocity and reflectivity factors. Gradients of reflectivity factor in the azimuthal and vertical direction have no effect on the Doppler spectrum width.

Gradients of reflectivity factor along the radial, and radial velocity along the radial, have little effect. This is fairly obvious when one considers that there will be little difference between values, even with large gradients, over the pulse depth of 150 m. Velocity shears in either the azimuthal or vertical transverse directions may significantly broaden the Doppler spectrum.

Further, the Doppler spectrum width provides a means of estimating the turbulence eddy dissipation rate, and a mapping of this quantity through a storm region. However, the estimates of $\epsilon^{1/3}$ derived from the Doppler spectrum width here are considerably larger than those estimated from aircraft data, which is an indication that other significant factors may be influencing the Doppler spectrum width, or that the assumption of the structure of the turbulence field is in error.

Some improvement to the radar estimates of the turbulence dissipation rate can be achieved by the removal of gradient effects from the Doppler spectrum width. While results indicate that such corrections to the radar-estimated turbulence dissipation rate may be

measurable, these corrections appear small in comparison to the large overestimates produced by the error sources in the variance estimates. Although corrections for gradient effects at short ranges are not significant, theoretical results indicate that such corrections may be very important at longer ranges.

In consideration of use for real-time hazard identification, rapid advection and evolution of storm features may make it difficult to determine atmospheric turbulence for a specific aircraft track. It may be more productive to map a statistical description of the turbulent field (i.e., maximum intensities and frequency-distributions) when attempting to warn pilots of turbulent conditions.

ACKNOWLEDGEMENTS

The author wishes to express his sincere thanks to the many individuals who assisted in the preparation of this report. Lincoln Laboratory (MIT) provided the aircraft and radar data tapes, and the algorithms and programs for decoding the tapes. Dr. Alan R. Bohne, Dr. F. Ian Harris, and Dr. James I. Metcalf (Air Force Geophysics Laboratory, Ground-based Remote Sensing Branch) provided invaluable assistance throughout the preparation period, and editorial guidance. Dr. Richard E. Passarelli, Jr. (Massachusetts Institute of Technology, Meteorology and Physical Oceanography Center) suggested the main theme of the research and provided the best of guidance. Lastly, my sincere thanks to Liz Manzi for the typing and preparation of the final report.

BIBLIOGRAPHY

1. Glossary of Meteorology, edited by Ralph E. Huschke, (Amer. Meteorological Soc., Boston, MA, 1959), pp 266, 631.

2. Rogers, R.R., and B.R. Tripp, 1964: Some radar measurements of turbulence in snow, J. Appl. Met. Vol. 3: 603-610.

3. Sloss, P.W. and D. Atlas, 1968: Wind shear and reflectivity gradient effects on Doppler radar spectra. J. Atmos. Sci., Vol. 25, 1080-1089.

4. Atlas, D., R.C. Srivastava, and P.W. Sloss, 1969: Wind shear and reflectivity gradient effects on Doppler radar: II, J. Appl. Met., Vol. 8, 384-388.

5. Frisch, A.S., and S.F. Clifford, 1974: A study of convection capped by a stable layer using Doppler radar and acoustic echo sounders. J. Atmos. Sci., Vol. 31, 1622-1628.

6. Frisch, A.S., and R.G. Strauch, 1976: Doppler radar measurements of eddy dissipation rates in a northeastern Colorado convective storm. J. Appl. Met., Vol. 15, 1012-1017.

7. Bohne, A.R., 1981: Radar detection of turbulence in thunderstorms, AFGL-TR-81-0102. (date of report 31 Mar 1981)

8. Bohne, A.R., 1982: Radar detection of turbulence in precipitation environments, J. Atmos. Sci., Vol. 39, 1819-1837.

9. Tennekes, H., and J.L. Lumley, A First Course in Turbulence, (MIT Press, Cambridge, MA, 1972), pp 1-3, 10-21.

10. MacCready, P.B. Jr., 1964: Standardization of gustiness values from aircraft, J. Appl. Met., Vol. 3, 439-449.

11. Batchelor, G.K., Theory of Homogeneous Turbulence, (Cambridge University Press, N.Y., 1959), pp 1-3.

12. Labbitt, M., 1981: Coordinated radar and aircraft observations of turbulence, ATC-108, MIT Lincoln Laboratory, Lexington, MA. (Prepared for FAA Systems Research and Development Service.)

13. Doviak, R.J., D.S. Zrnic, and D.S. Sirmans, 1979: Doppler weather radar, Proceedings of the IEEE, Vol. 67, Vo 11, 1522-1553.

14. Gradsteyn, I.S., and I.M. Ryzhik, Table of Integrals, Series and Products, (Academic Press, NY, 1965), pp 92, 307, 337.

FOR GRADIENTS:				SPECTRUM WIDTH DUE TO GRADIENTS:		
K1	K2	K3	B3	25.0km	50.0km	75.0km
(	m/sec/km	)	(dBz/km)	(	m/sec	)
0.0	0.0	0.0	0.0	0.000	0.000	0.000
0.0	0.0	0.0	5.0	0.000	0.000	0.000
0.0	0.0	0.0	10.0	0.000	0.000	0.000
0.0	0.0	0.0	20.0	0.000	0.000	0.000
0.0	0.0	5.0	0.0	0.217	0.217	0.217
0.0	0.0	10.0	0.0	0.433	0.433	0.433
0.0	0.0	20.0	0.0	0.866	0.866	0.866
0.0	0.0	5.0	10.0	0.216	0.216	0.216
0.0	0.0	10.0	10.0	0.432	0.432	0.432
0.0	0.0	20.0	20.0	0.856	0.856	0.856
0.0	5.0	0.0	0.0	0.983	1.965	2.948
0.0	10.0	0.0	0.0	1.965	3.931	5.896
5.0	0.0	0.0	0.0	0.983	1.965	2.948
10.0	0.0	0.0	0.0	1.965	3.931	5.896
5.0	5.0	0.0	0.0	1.390	2.779	4.169
5.0	10.0	0.0	0.0	2.197	4.395	6.592
10.0	10.0	0.0	0.0	2.779	5.559	8.338
5.0	5.0	5.0	5.0	1.406	2.788	4.175
5.0	5.0	10.0	10.0	1.455	2.813	4.191
10.0	10.0	10.0	10.0	2.815	5.576	8.349

Table 1: Representative values of gradient effects on Doppler spectrum width. (Assumed beamwidth - 1.5°, pulse depth = 150m)

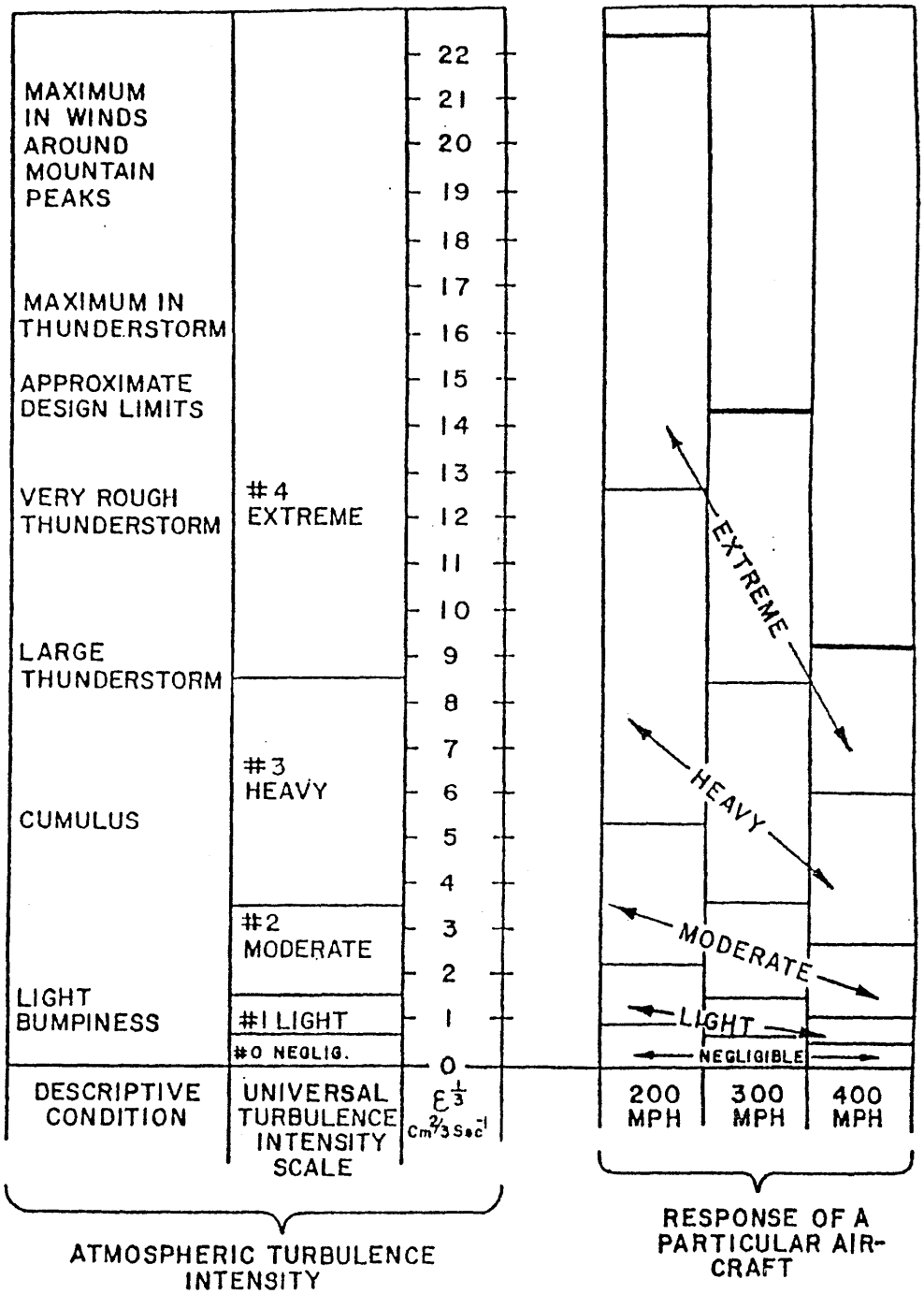

Figure 1. Aircraft Turbulence Intensity Scale correlated with Turbulence Eddy dissipation rate ($\varepsilon^{1/3}$). (Source: MacCready, 1964)

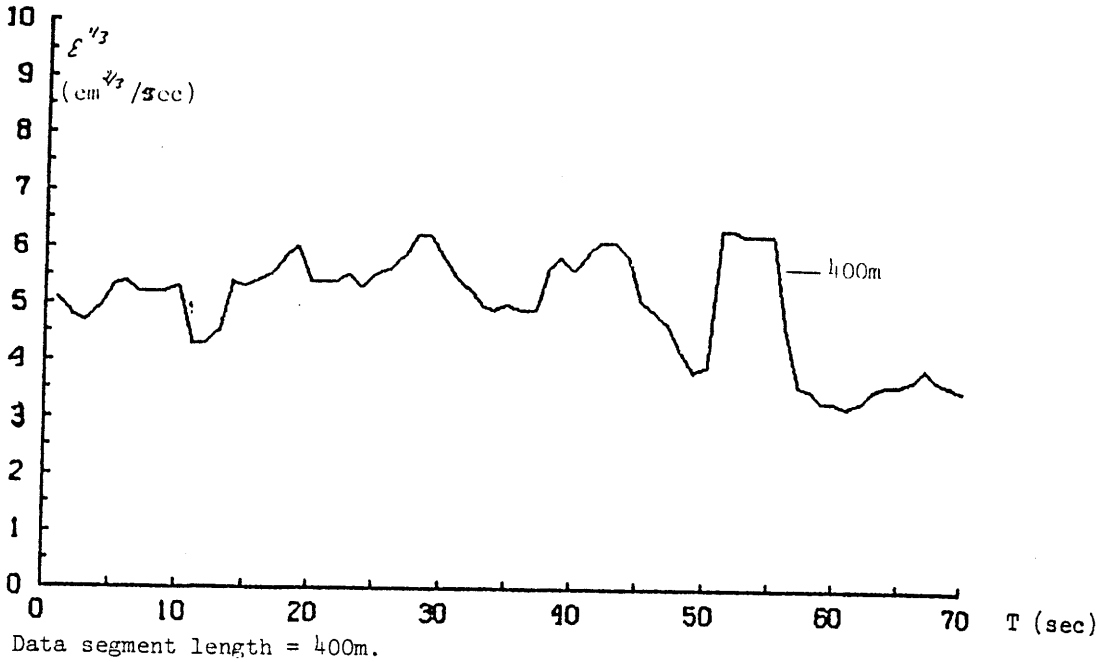

Data segment length = 400m.

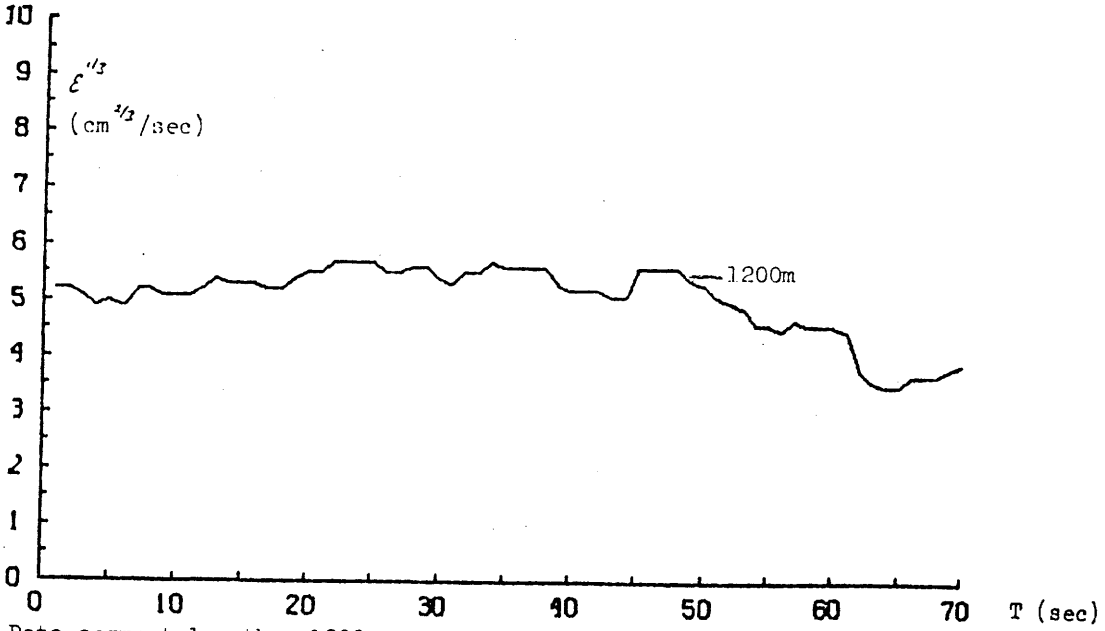

Data segment length = 1200m.

Figure 2. Time histories of $\varepsilon^{1/3}$ (cm$^{2/3}$/sec) for data segment lengths of 400m and 1200m for the same time interval.

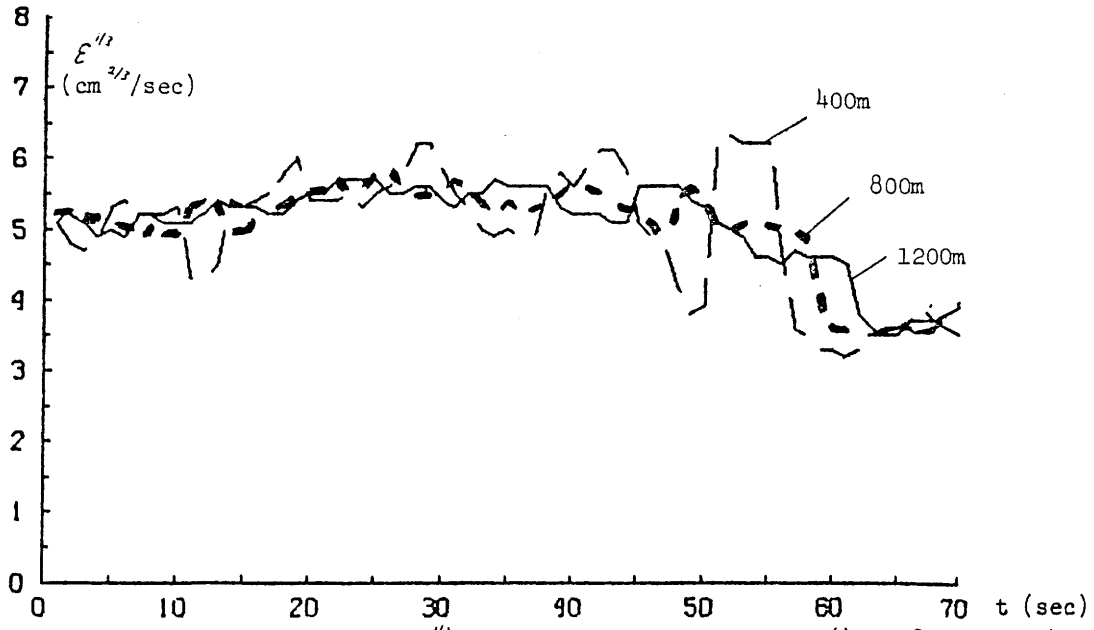

Figure 3. Time histories of $\varepsilon^{1/3}$ for 3 data-segment lengths (400, 800, 1200m) superimposed. (Large dash = 400m, small dash = 800m, solid = 1200m).

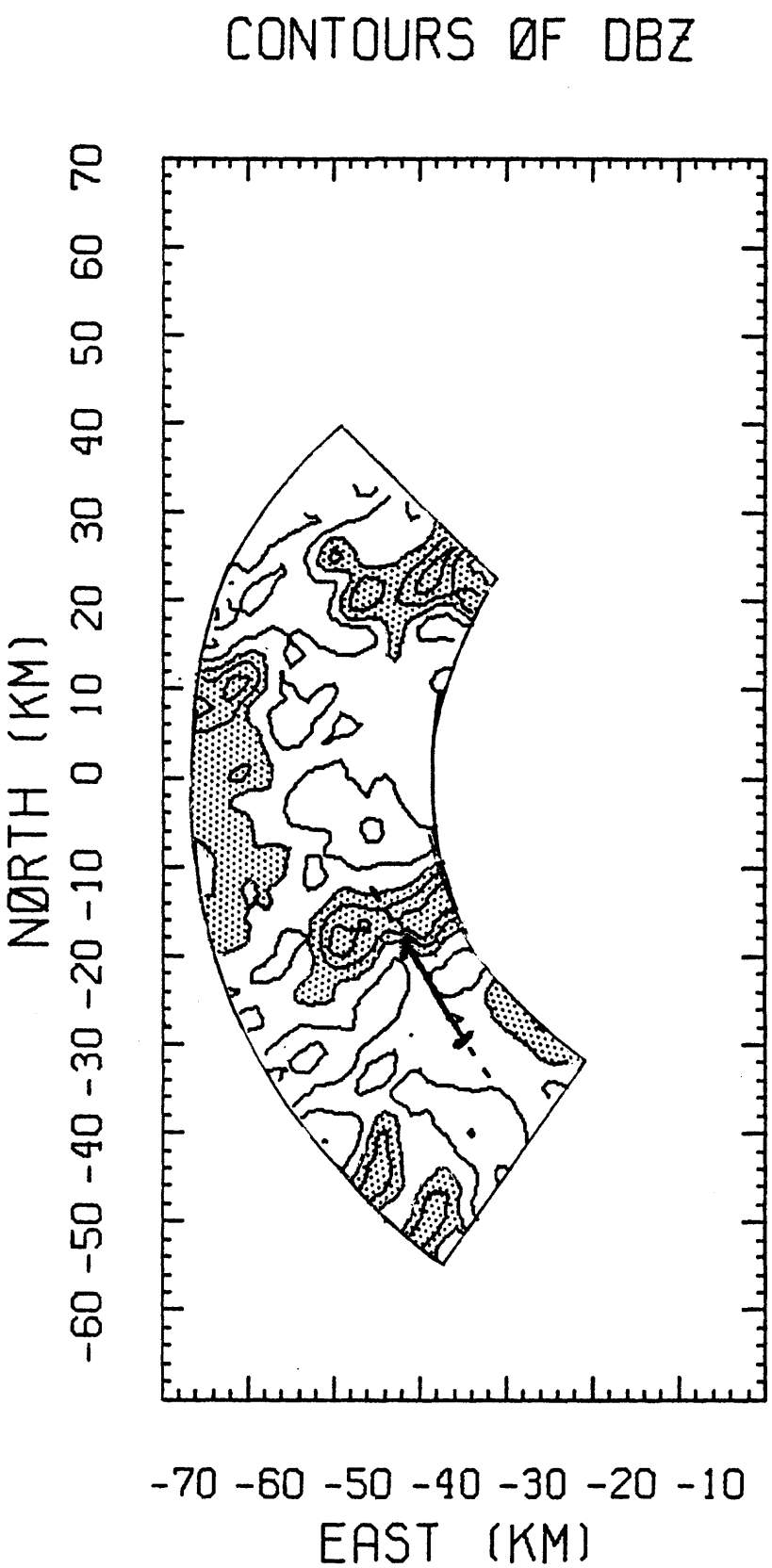

Figure 4. Reflectivity factor field at 2km, morning run. Aircraft track is indicated. Contour interval = 4 dBz, stippling indicates >28 dBz.

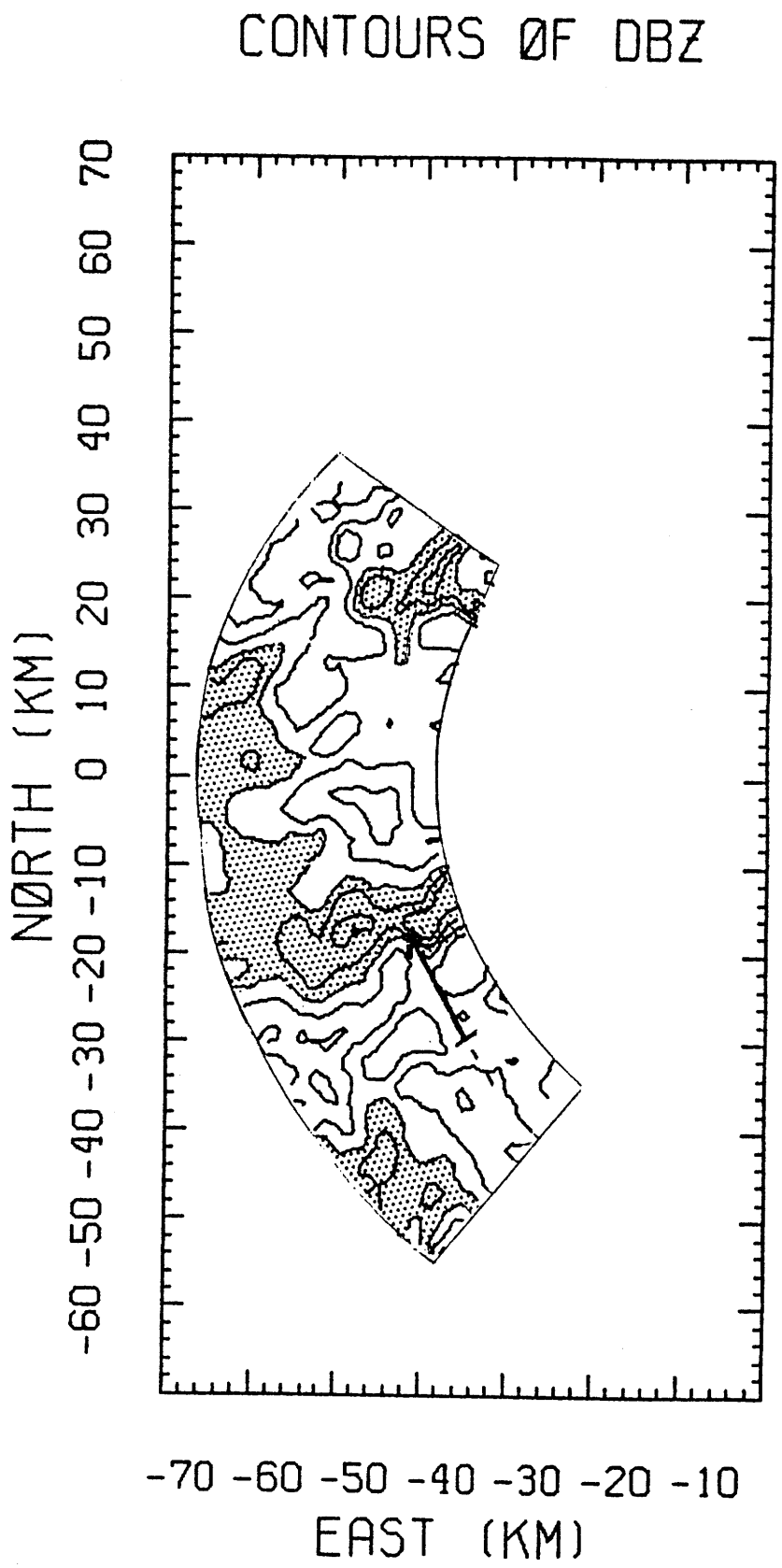

Figure 5. Reflectivity factor field at 3km, morning run. Aircraft track is indicated. Contour interval = 4 dBz, stippling indicates >28 dBz.

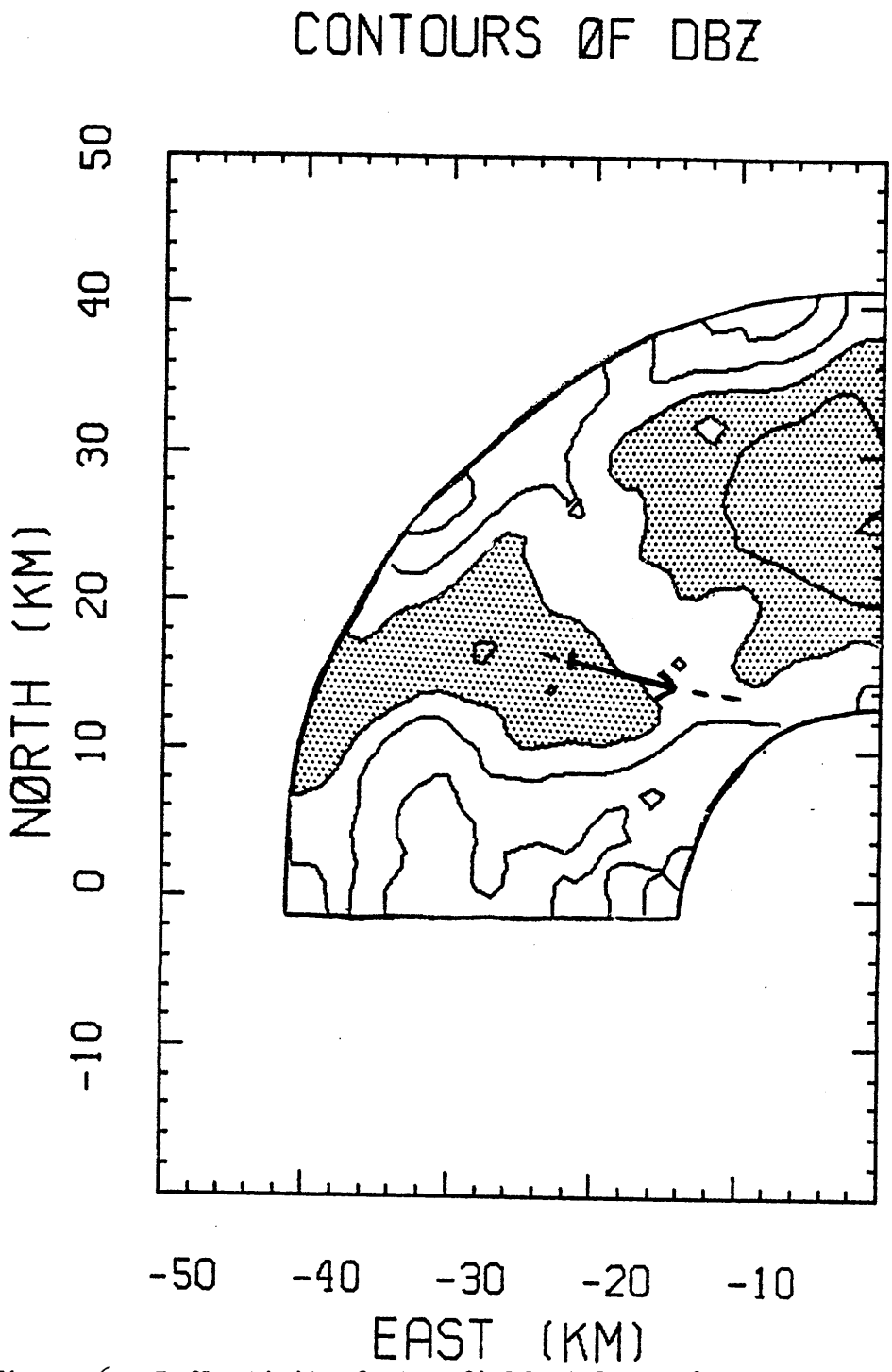

Figure 6. Reflectivity factor field at 1km, afternoon run. Aircraft track is indicated. Contour interval = 4 dBz, stippling indicates >28 dBz.

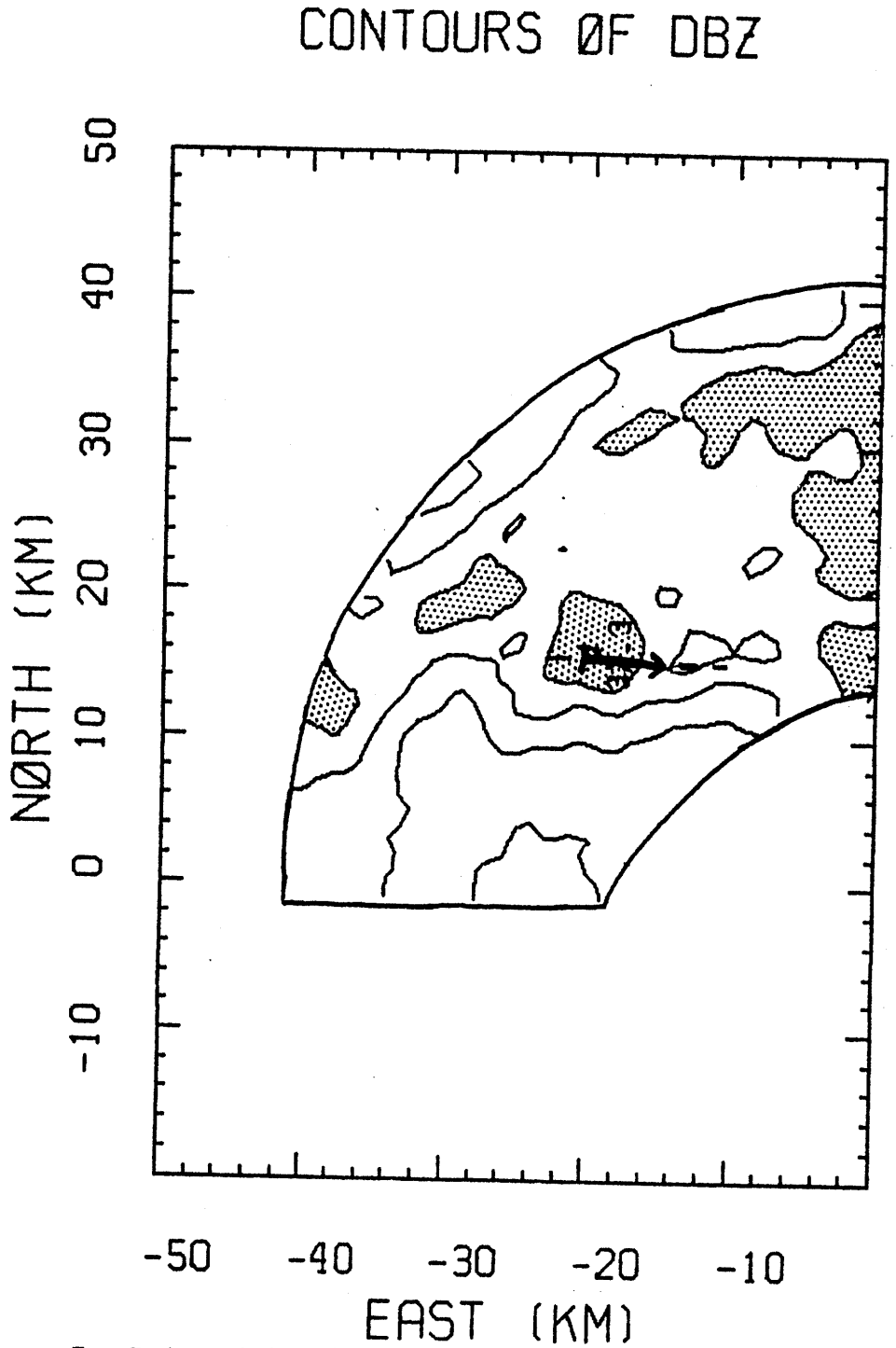

Figure 7. Reflectivity factor field at 2km, afternoon run. Aircraft track is indicated. Contour interval = 4 dBz, stippling indicates >28 dBz.

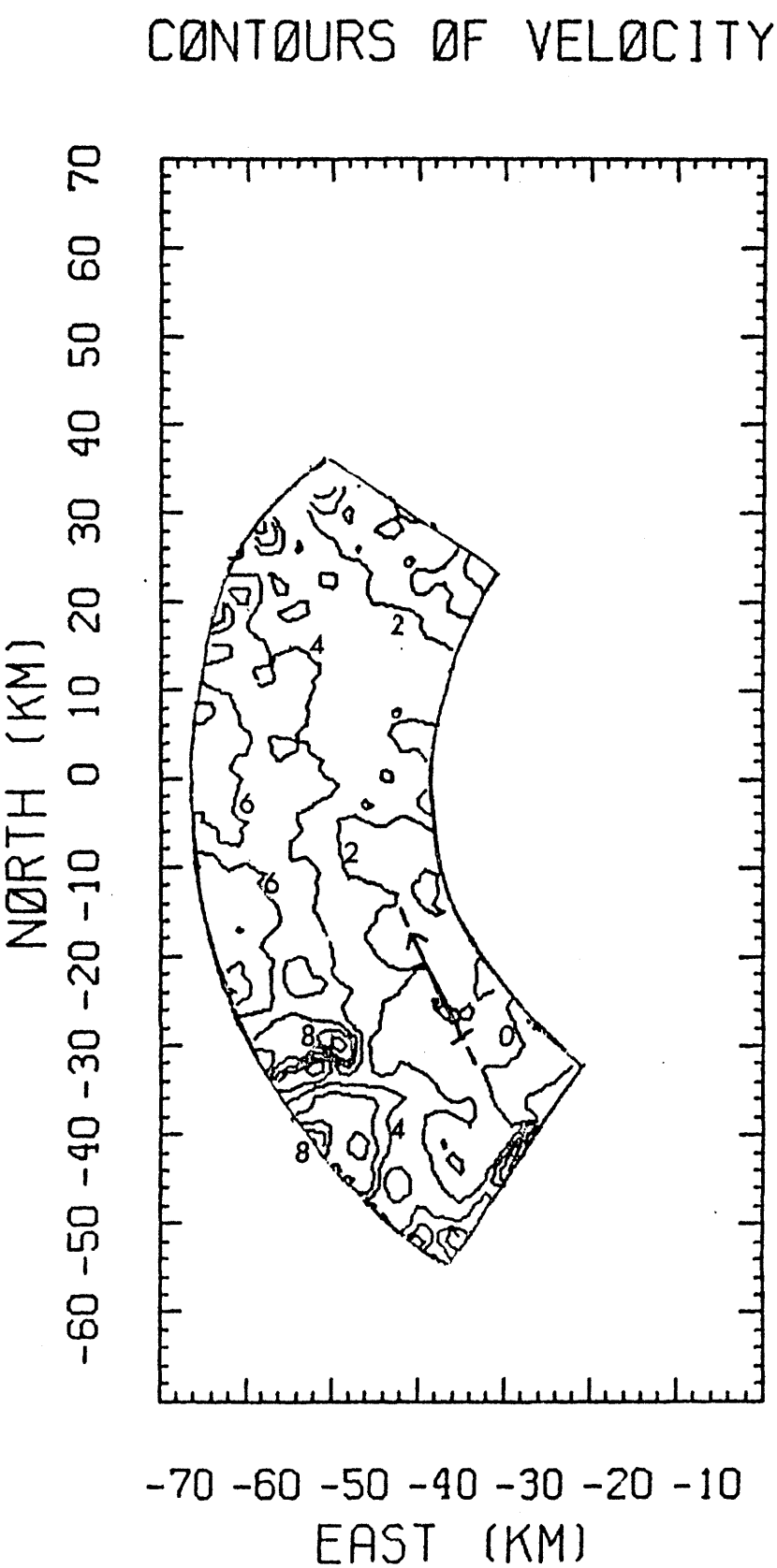

Figure 8. Radial velocity field at 2km, morning run. Aircraft track is indicated. Contour interval = 2 m/sec, v>o is towards radar.

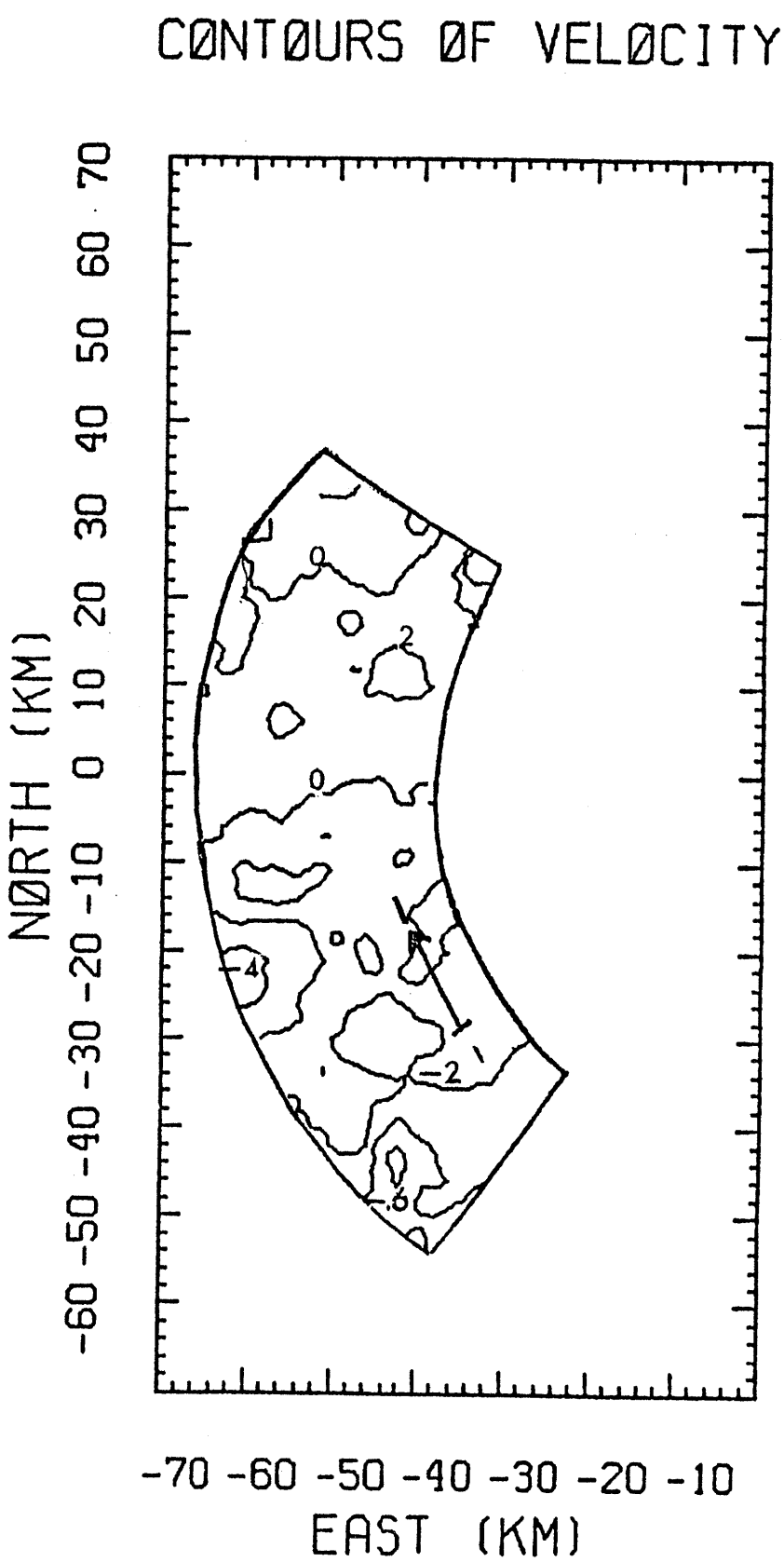

Figure 9. Radial velocity field at 3km, morning run. Aircraft track is indicated. Contour interval = 2 m/sec, v>o is towards radar.

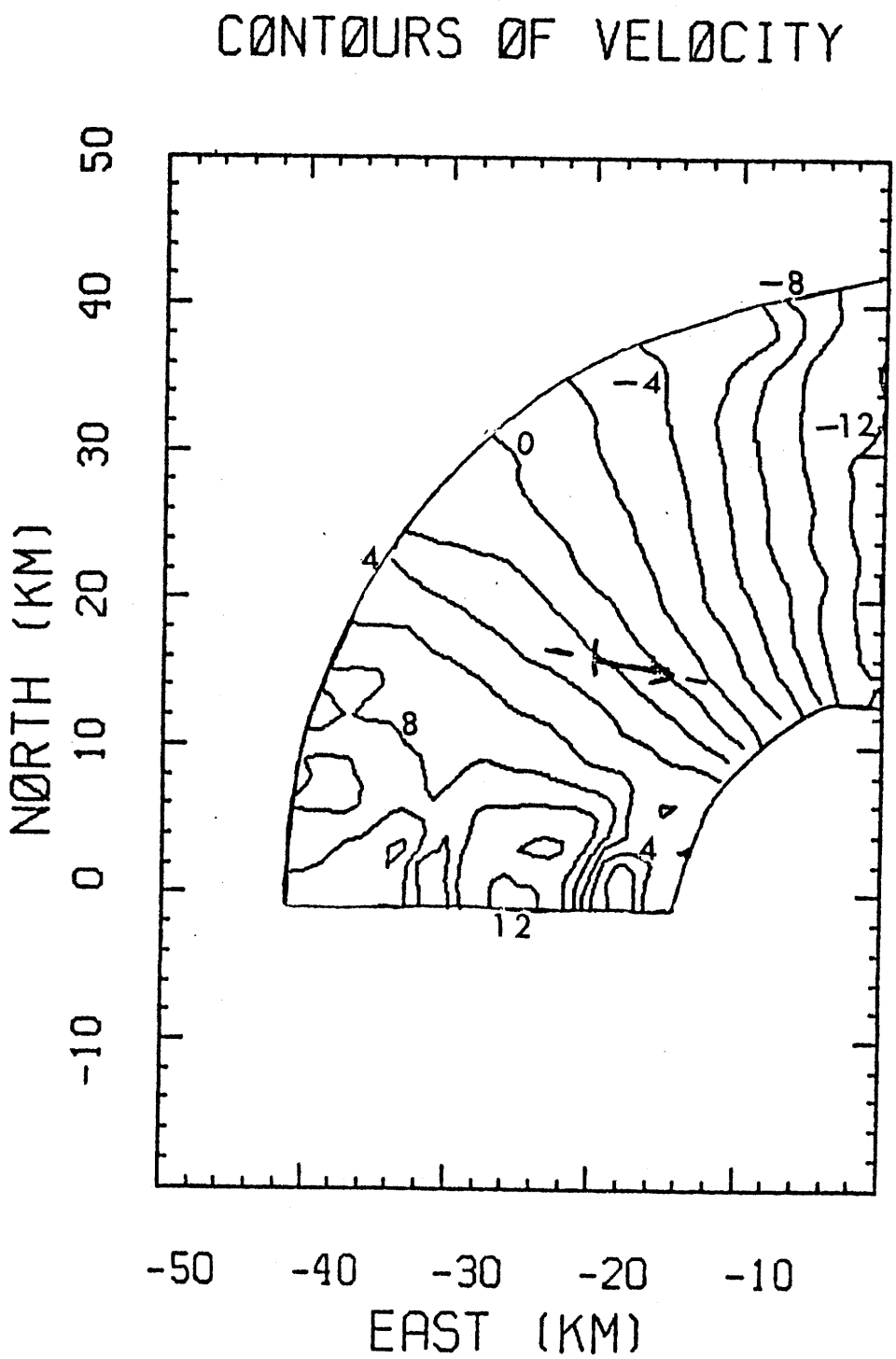

Figure 10. Radial velocity field at 1km, afternoon run. Aircraft track is indicated. Contour interval = 2 m/sec, v>o is towards radar.

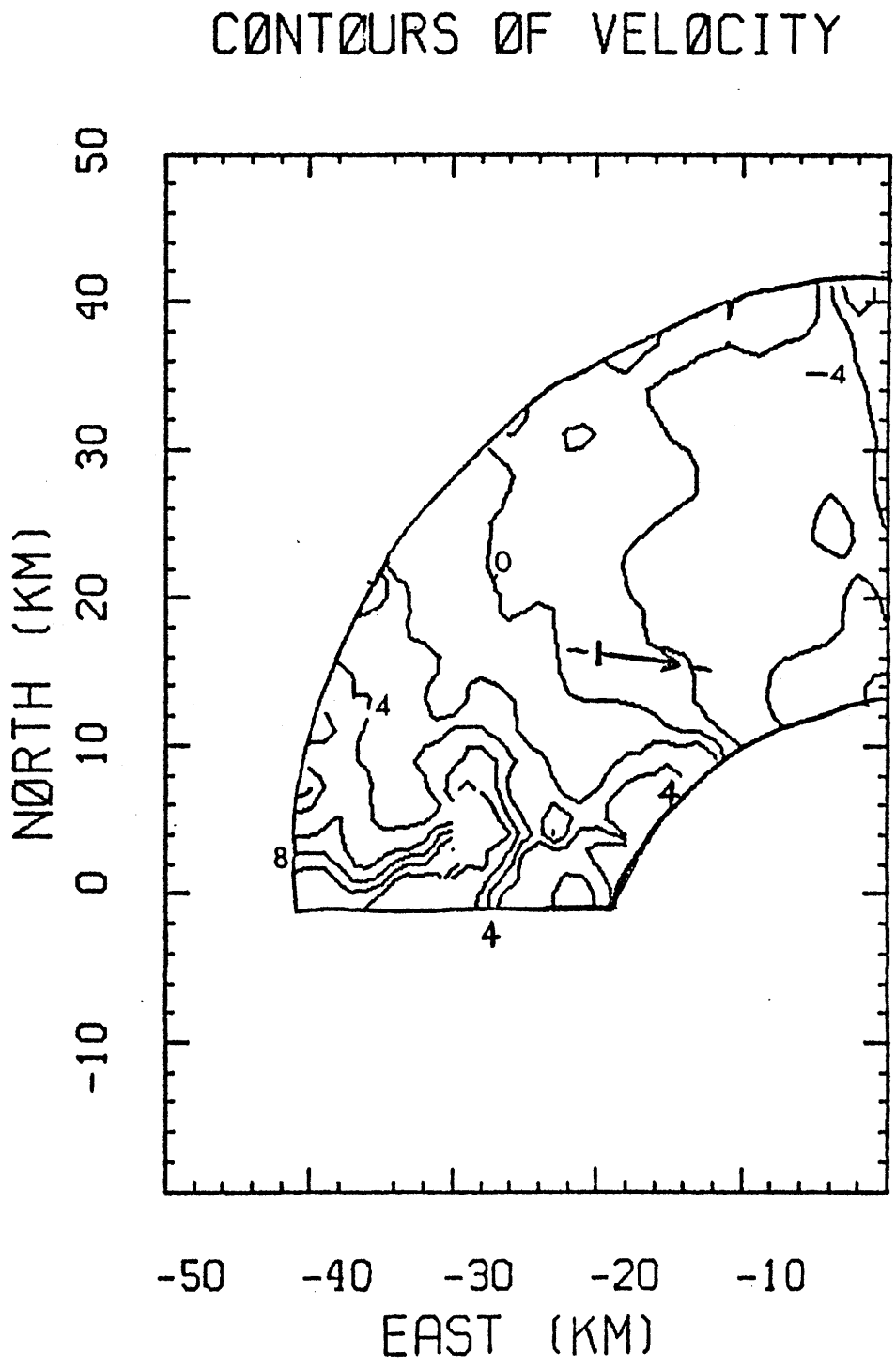

Figure 11. Radial velocity field at 2km, afternoon run. Aircraft track is indicated. Contour interval = 2 m/sec, v>o is towards radar.

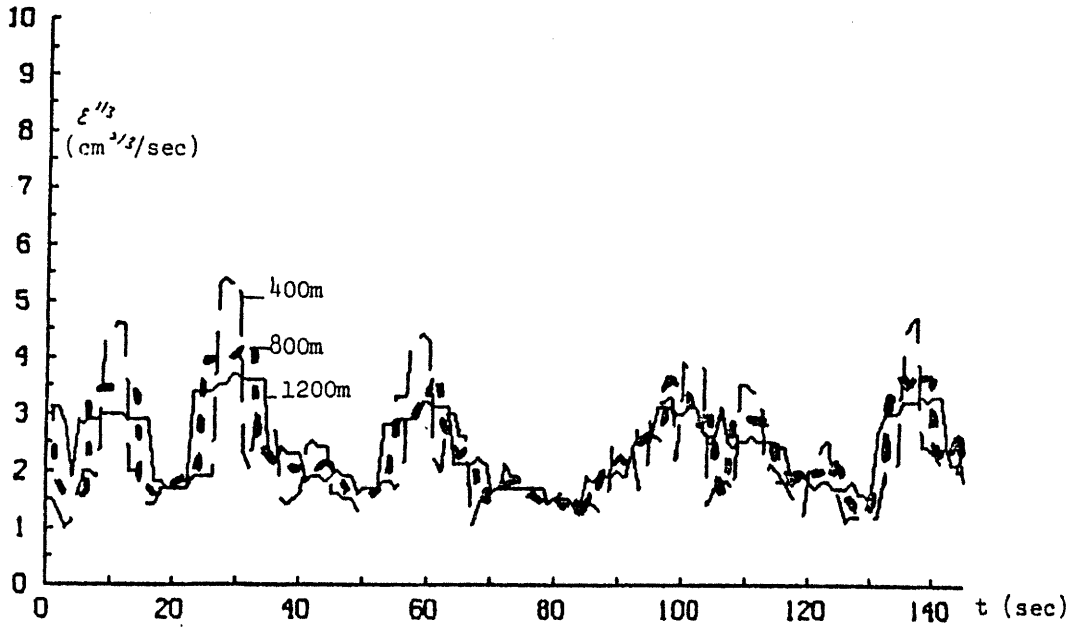

Figure 12. Time history of aircraft-estimated $\varepsilon^{1/3}$ (cm$^{2/3}$/sec) for morning aircraft run. (Large dash = 400m, small dash = 800m, solid = 1200m)

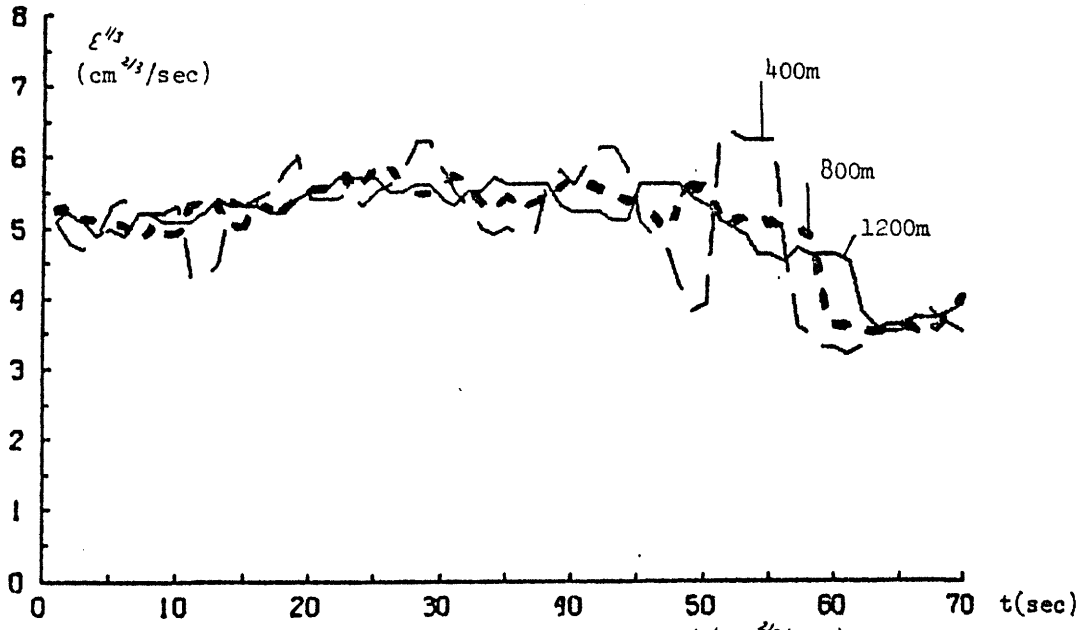

Figure 13. Time history of aircraft estimated $\varepsilon^{1/3}$(cm$^{2/3}$/sec) for afternoon run. (Large dash = 400m, small dash = 800m, solid = 1200m).

Figure 14: Block diagram of data processing scheme.

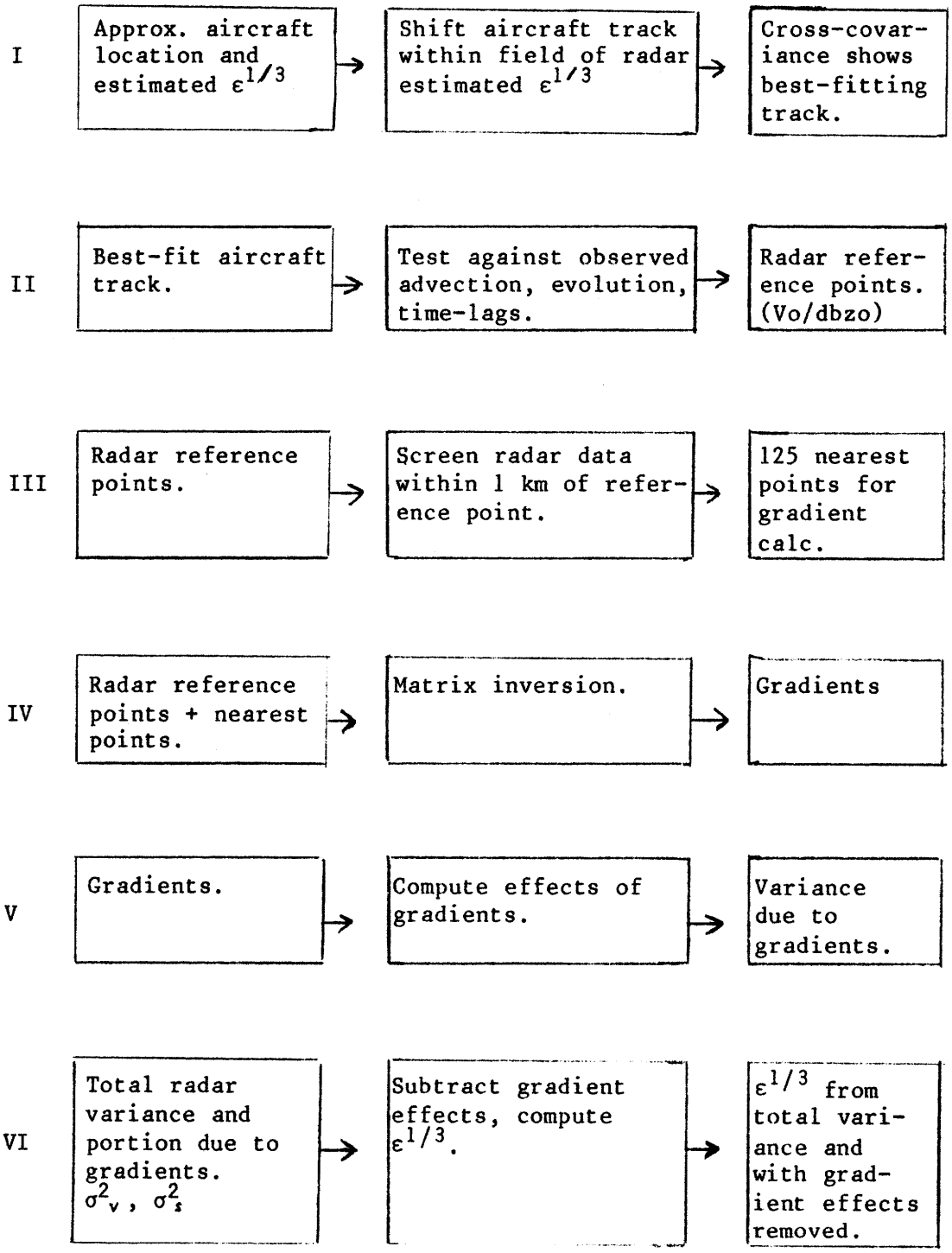

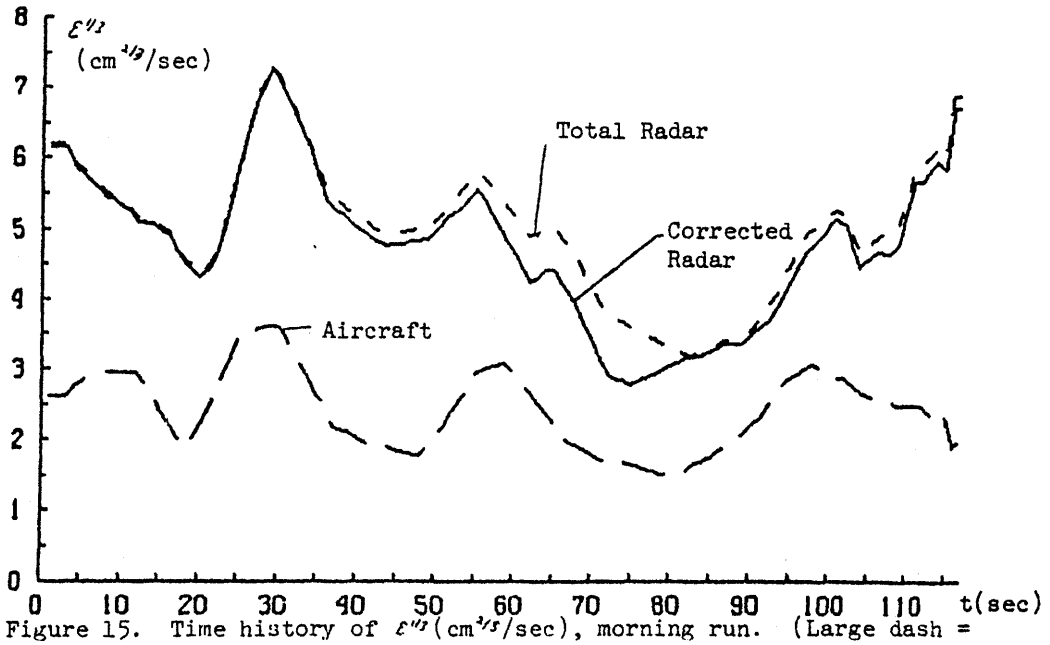

Figure 15. Time history of $\varepsilon^{1/3}$(cm$^{2/3}$/sec), morning run. (Large dash = aircraft, small dash = radar without gradient effects removed, solid = radar with gradient effects removed.

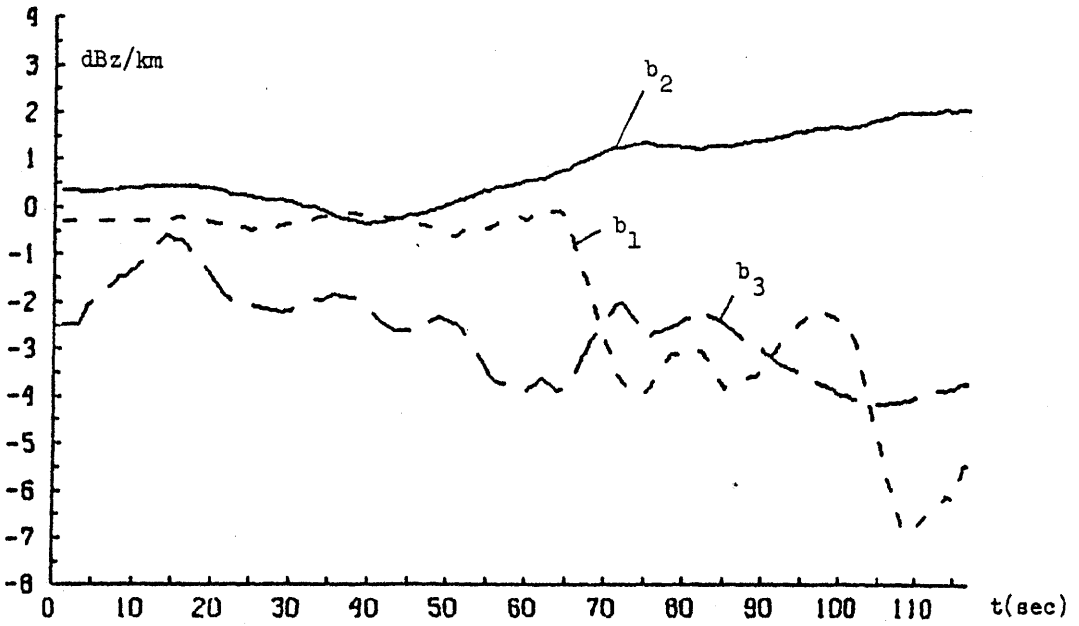

Figure 16. Time history of reflectivity factor gradients (dBz/km), morning run. (Large dash = radial (b_3), small dash = vertical (b_1), solid = azimuthal (b_2)).

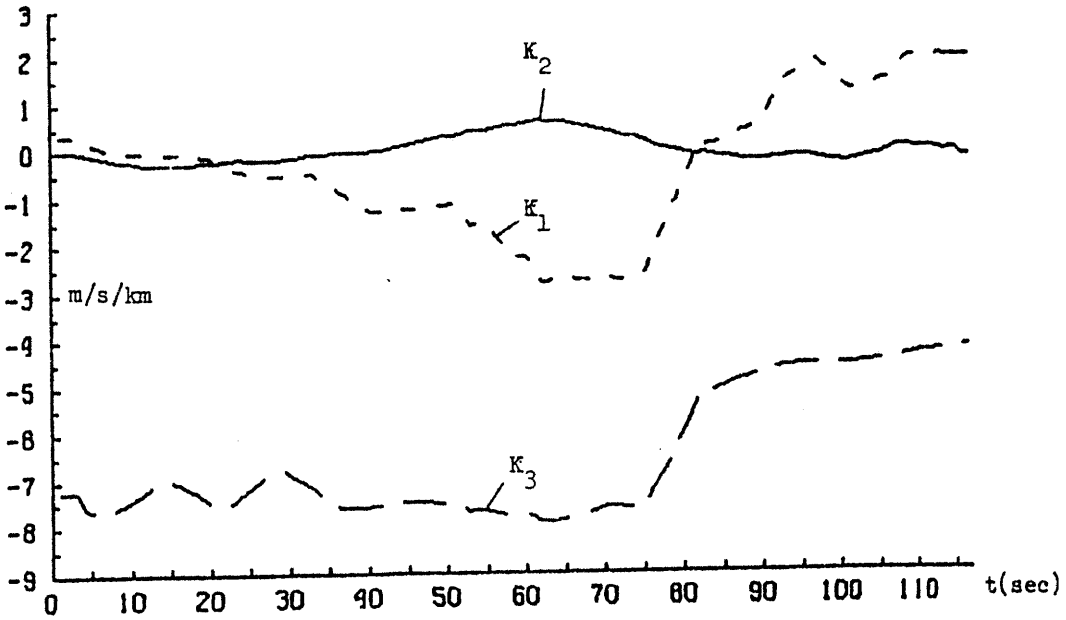

Figure 17. Time history of radial velocity shears (m/sec/km), morning run. (Large dash = radial (K_3), small dash = vertical (K_1), solid = azimuthal (K_2)).

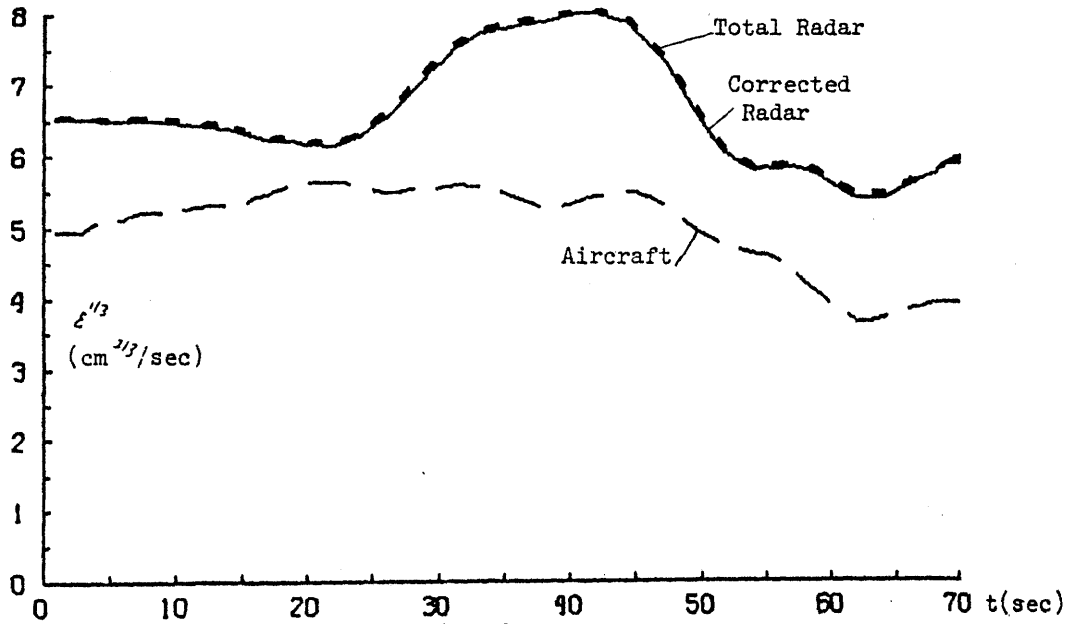

Figure 18. Time history of $\varepsilon^{1/3}$(cm$^{2/3}$/sec), afternoon run. (Large dash = aircraft, small dash = radar without gradient effects removed, solid = radar with gradient effects removed).

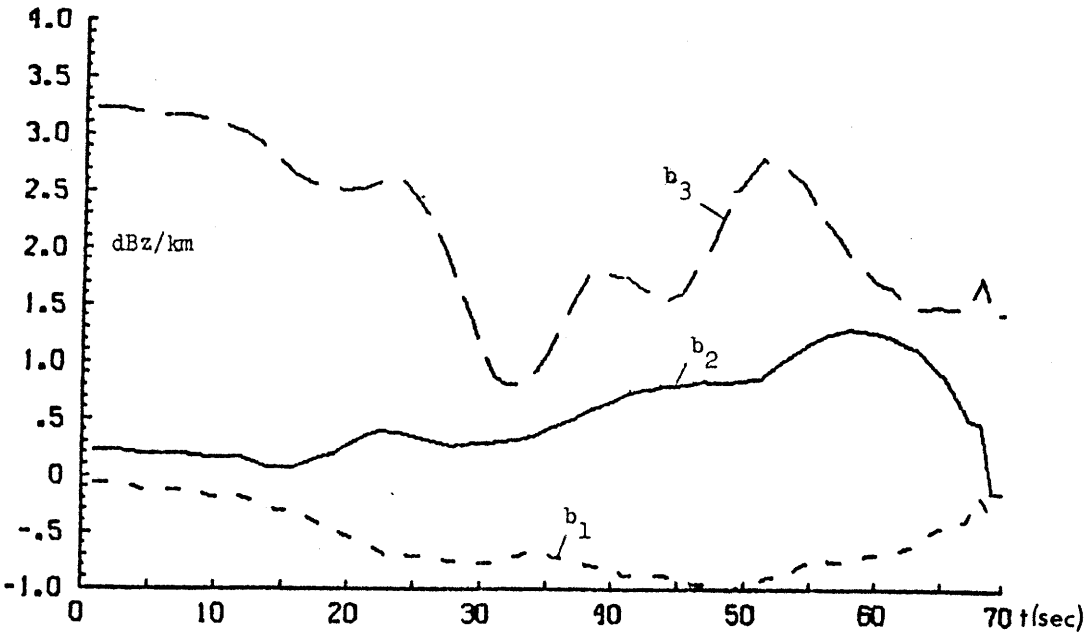

Figure 19. Time history of reflectivity factor gradients (dBz/km), afternoon run. (Large dash = radial (b_3), small dash = vertical (b_1), solid = azimuthal (b_2)).

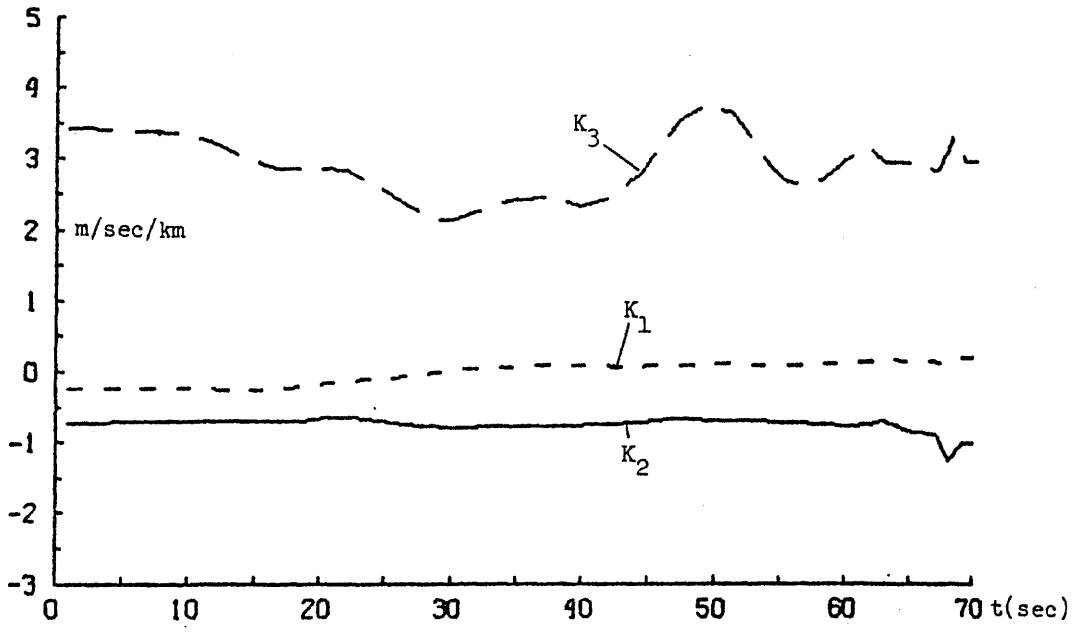

Figure 20. Time history of radial velocity shears (m/sec/km), afternoon run. (Large dash = radial (K_3), small dash = vertical (K_1), solid = azimuthal (K_2)).

APPENDIX A

MIT TESTBED RADAR CHARACTERISTICS

Antenna

Aperture	18 feet
Gain	42 dB
Sidelobe Levels	-26 dB minimum
Beamwidth	1.45° one-way
Polarization	horizontal
Maximum rotation rate	6 r.p.m. (both axes)
Height	312 ft. above m.s.l.

Transmitter

Source	VA87 klystron
Frequency	2705 MHz
Peak Power	1 MW
Pulse Width	1 microsecond
P.R.F.	Variable (1200 Hz max.)

Receiver

Pre-selector	tunable cavity
RF amplifier	solid state
Noise figure	4 dB
STALO	crystal controlled
COHO	30 MHz crystal
Bandwidth	1.1 MHz
STC	PIN diode at RF
STC curve	Range squared
M.D.S.	-103 dBm

Digital Signal Processor

A/D Converters	12 bits I; 12 bits Q
Range sample spacing	1/16,1/8,1/4,1/2 n.m.
Number of range gates processed	288
Algorithm	pulse-pair processing
Processor output	0th, 1st, 2nd moments
Clutter filter	Optional block-MLS

Radar Location

Latitude	42° 21' 36"
Longitude	71° 5' 25"

APPENDIX B

BASIC EQUATIONS AND ALGORITHMS USED IN DECODING RADAR DATA TAPES

Given quantities:

p = radar PRF (Hz)
λ = radar wavelength (meters)
N_r = receiver noise (same units as R_o)

r = slant range (meters)
R_o = "zeroth lag" (unnormalized)
R_1 = "first lag" (unnormalized)
R_2 = "second lag" (unnormalized)

Computed quantities:

$\hat{N}_s$ = estimated signal noise (R_o units)
$\hat{S}$ = estimated S/N ratio (dB)
$\hat{R}$ = estimated reflectivity (dBZ)
$\hat{V}$ = estimated Doppler velocity (meters/sec.)
$\hat{W}$ = estimated spectrum width (meters/sec.)

Basic equations:

(1) $$\text{S/N ratio} = \left[\frac{R_0 |R_2|^{1/3}}{|R_1|^{4/3}} - 1 \right]^{-1}$$

(2) $$\hat{N}_s = \frac{R_s}{1 + S/N} = R_0 - \frac{|R_1|^{4/3}}{|R_2|^{1/3}}$$

(3) $$\hat{S} = 10 \log_{10} \left[\frac{R_0 - \hat{N}_s}{N_s} \right]$$

(4) $$\hat{R} = 10 \log_{10} \left[\left(\frac{R_0 - \hat{N}_s}{N_r} \right) \left(\frac{r}{25000} \right)^2 \right]$$

(5) $$\hat{V} = \frac{\lambda}{4\pi} p \, \text{Arg}[R_1]$$

(6) $$\hat{W} = \frac{\lambda^2 p^2}{24 \pi^2} \ln \left(\frac{|R_1|}{|R_2|} \right)$$

Suggested algorithm:

(1) Compute N_s and S:

Two cases:

($|R2| = Q$): $\hat{N}_s = 0, \quad S = +100$

($|R2| > 0$): $T1 = R_o - (|R1|^4/|R2|)^{1/3}$

Three cases:

($T1 < 0$): $\hat{N}_s = N_r$
$\hat{S} = 10 \log_{10}((R_o - \hat{N}_s)/\hat{N}_s)$

($0 \leq T1 < R_o$): $\hat{N}_s = T1$
$\hat{S} = 10 \log_{10}((R_o - \hat{N}_s)/\hat{N}_s)$

($T1 \geq R_o$): $\hat{N}_s = R_o$
$\hat{S} = -100$

(2) Compute $\hat{R}$:

Two cases:

($S \leq 0$): $\hat{R} = -100$

($S > 0$): $\hat{R} = 10 \log_{10}\left[\frac{(R_o - \hat{N}_s)}{N_r}\left(\frac{r}{25000}\right)^2\right]$

(3) Compute $\hat{V}$:

Two cases:

($\hat{S} \leq 5$) $\hat{V} = 0$

($\hat{S} > 5$) $\hat{V} = \lambda/4\pi \; P \; \mathrm{Arg}[R1]$

(4) Compute $\hat{W}$:

Two cases:

($\hat{S} \leq 10$): $\hat{W} = 0$

($\hat{S} > 10$): three cases:

($|R1| \leq |R2|$): $\hat{W} = 0$

($|R2| = 0$): $\hat{W} = 100$

($|R1| > |R2| > 0$): $\hat{W} = \lambda^2 P^2 / 24\pi \ln(|R1|/|R2|)$

For MIT WR66L data:

$h = 0.11$ meters
$N_r = 60$ "counts"

APPENDIX C

A TECHNIQUE TO CO-LOCATE AIRCRAFT AND RADAR DATA

It is extremely difficult to co-locate and correlate aircraft and radar data points spatially and temporally, and basically impossible if the instruments measuring the aircraft or radar location are inaccurate. The problem is compounded even further if storm features are evolving rapidly, or are experiencing large advections. These problems appeared in the analysis of the data for August 12, 1983. It was virtually impossible to obtain any reasonable correlation between the two data sets by simply seeking radar reference points close to the reported aircraft positions. An alternative method of selecting radar data reference points is described.

The radar estimated energy dissipation rates for the entire field traversed by the aircraft are interpolated to a plane at the altitude of the aircraft. The aircraft track is shifted through the radar data field, with shifts up to 3 kilometers north, south, east, and west from the original reported starting point of the track, in increments of .25 kilometers. The track is allowed to veer from the original heading, beginning at the new starting point, with angular shifts up to 15°, in 1 degree increments.

The cross-covariance of the radar-estimated $\varepsilon^{1/3}$ (interpolated to the plane) and the aircraft-estimated $\varepsilon^{1/3}$ is computed

for each aircraft track placed in the radar data-plane. The higher covariance values associated with a set of closely spaced tracks indicates the "best-fit" of aircraft and radar data.

The track providing the best fit is then plotted against the nominal track originally indicated. The additional factors of advection, evolution, and the difference between time of aircraft passage and time of radar observation are considered. In the case of both runs on August 12, winds from the south-southwest at approximately 30 knots and the time differential between the data sets made an apparent shift to the north and east of 2.5 km in each direction from the original starting point necessary. Angular shifts of 3-5° from the original heading in a counterclockwise direction yielded better cross-covariance values (>.6) for the morning run. Best cross-covariance values (>.6) for the afternoon run were achieved without angular shifts from the original heading (a set of tracks within 1° of the original heading provided similar values).

It is assumed that the shifted aircraft track compensates for the inaccuracies in the aircraft or radar locations and for motion and evolution of the field, so that the shifted aircraft track provides the best source of radar data points. The radar reference points (Vo, dBZo, $\epsilon^{1/3}$) are selected from that track. After this selection of data points is accomplished the data are processed for radial velocity and reflectivity factor gradient effects.

The problems described above imply that it may be difficult to give accurate turbulence warnings to aircraft pilots. It appears

that a specific track analysis will not be useful, if the field within the track changes rapidly. A useful alternative may be a statistical description of the large scale field (i.e., by quadrants), where the maximum and mean values and a description of the frequency distribution could be provided.